THERMALLY INDUCED POLYMER DEFORMATION FOR ADAPTIVE OPTICS

THERMALLY INDUCED POLYMER DEFORMATION FOR ADAPTIVE OPTICS

BY

LEI WANG

B. SC.

SUBMITTEDTOTHE MATERIALS SCIENCE & ENGINEERING

AND THE SCHOOL OF GRADUATE STUDIES

OF MCMASTER UNIVERSITY

IN PARTIAL FULFILMENT OF THE REQUIREMENTS

FOR THE DEGREE OF

MASTER OF APPLIED SCIENCE

MASTER OF APPLIED SCIENCE (2015) McMaster University

Department of Materials Science and Engineering Hamilton, Ontario

TITLE: Thermally induced polymer deformation for adaptive optics

AUTHOR: Lei Wang

B. Sc. (Material Chemistry)

University of Jinan, Jinan, China

SUPERVISOR: Dr.Adrian Kitai

NUMBER OF PAGES: xii, 90

Abstract

Research on novel solar tracking methods using two polymer-based approaches was conducted. The first design for a solar tracking system with luminescent particles moving along polymer coatings is reported to provide the localized absorption of sunlight by phosphors which can follow the sun and hence provides a higher light intensity to be guided to a solar cell with higher efficiency. The second approach for realizing a polymer-based deformable lens on the surface of patterned ITO glass for light concentrating is reported. Both approaches rely on the application of spatially defined heating to a diluted polymer. These experiments were motivated by a) the well-known Rayleigh-Bénard convection flow within a fluid and b) Bénard-Marangoni flow effects concerning the movement of liquid along the surface of the fluid based on a surface tension gradient as a function of temperature.

In the first project, luminescent particles (YAG:Ce) are placed on the surface of a polymer film cast from a hot melt glue stick with a low melting point. When a heating wire 0.5 mm away from the top surface of the polymer film sample is transferred across the polymer, the floating YAG:Ce particles on the polymer surface can be pushed forward. In order to understand the mechanism of the particle movement, a laser-based measuring method was developed to view the surface profile of the melting polymer in situ. The melted glue stick polymer is observed to form a valley-like surface cross section that is able to transport YAG:Ce powder particles much like a surfer is carried forward on a wave.

In the second project, a 0.25 mm thick polystyrene polymer containing a toluene solvent is cast on an ITO coated glass substrate with ITO stripe widths of 2, 6, and 10 mm. The heating source comprised of the ITO stripe can produce spatially selective heat when electric current is applied to thermally deform the cast polymer/solvent layer (polystyrene) on the substrate surface. After the deformation is complete an LED light source is used to determine the light concentration properties of the thermally formed lenses. The ITO stripe surface temperature profile was measured with a thermocouple and modelled with COMSOL Multiphysics software. The vaporization weight loss of solvent was also determined.

The optics of the LED light concentration was modelled by Optics Lab software. When the light emitted from the source passes through the thermally deformed polymer, focusing into two beams occurs in agreement with modelling results.

Acknowledgements

I would like to express my deepest gratitude and appreciation to my supervisor, Dr. Adrian Kitai for his guidance, encouragement and great support throughout the course of my master degree. I would also like to thank my colleagues for their support, helpful suggestions, and assistance. Thanks to Dr. John Vlachopoulos and Dr. Gyan Johari for the great help with the theory for my research, Dr. Michael A. Brook for the suggestion of the polymer materials selection, Dr. James Cotton for the support of thermal modelling.

I would appreciate the kind help from McMaster Manufacturing Research Institute (MMRI) for training me on several pieces of equipment. I would also like to thank all the help from the department of Materials Science and Engineering for the course of my graduate study and the assistance with my project.

Finally, I would also like to express my deepest gratitude and appreciation to my family and friends, especially my parents for always keeping me grounded, and providing needed support throughout my degree. A warm gratitude to my girlfriend, Wenwen Wang, her company and motivation always kept me moving forward.

Table of Contents

List of Figures

List of Tables

Chapter 1: Introduction

1.1 Background Information

Because the reality of diminishing fossil fuel is influencing more and more of normal life nowadays, governments and scientific research institutions worldwide have commenced towards renewable energy technologies and make more effort for the rising energy demand gap. Solar cells have attracted growing attention for their great application potential for residential and businesses markets as a source of economical and clean energy.

However, humans still show incapability to control and utilize this tremendous wealth given by nature for application purpose of heat, light and electricity. Solar energy only accounts for 0.17% of the global energy consumption by fuel in 2013 [1].

Currently, the cost of silicon-based photovoltaic (PV) cells remains relatively high [2]. In order to obtain substantial absorption of sunlight by an installed photovoltaic panel, huge area arrays of solar panels are widely established for the absorption of sunlight, as shown in Figure 1 [3].

Figure 1: Nellis Solar Power Plant in the United States [3].

For reducing the large usage and the high cost of solar panels, a solar tracker is currently applied, which tracks the position of the sun over the whole day, from sun rise to sun set. The tracker consists of solar panels, motors and mechanical systems with installation costs and high daily operating and maintenance expense, as shown in Figure 2 [4]. The aesthetics of solar tracking system make them undesirable for residential applications.

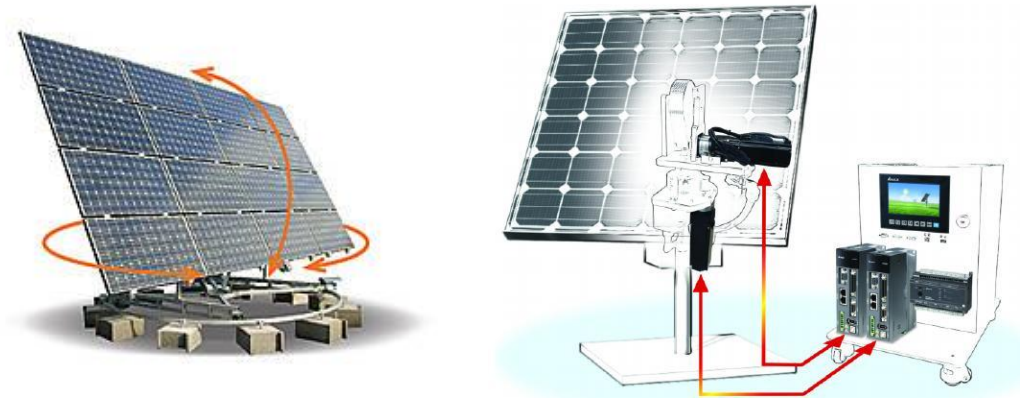

Figure 2: Operation of a solar tracker with the motor and mechanical system [4].

One solar system being developed for the purpose of lowering the usage area of solar cell/panel is the Fluorescent Solar Concentrator (FSCs) [5].

How a FSC works is now explained in detail. In one particular design of FSCs, it consists of a transparent substrate (known as waveguide), a luminescent dye or fluorescent material embedded in the substrate and solar cell attached at the edges. The luminescent materials (such as phosphors particles) are efficient to absorb and track sunlight over most of the solar spectrum and emit most of the absorbed energy as longer wave luminescence, which is conveyed to the solar cell attached at the edges of the whole FSCs device through the transparent waveguide after sunlight penetrates the top surface

of the transparent substrate [6]. More electricity will be converted if higher intensity of radiation can be conveyed to the solar cell, hence the absorption of light intensity by the luminescent particles must be improved.

With the random position of luminescent particles, the efficiency of waveguiding is compromised because of re-absorption losses of the longer wave luminescence by the fluorescent material.

In addition, a lens-based solar concentrator [7] can be applied as an alternative to replace and lower the expense of solar trackers, so as to decrease the cost of PV solar cell. The lens-based concentrator reduces re-absorption losses because a much reduced loading of fluorescent material is sufficient.

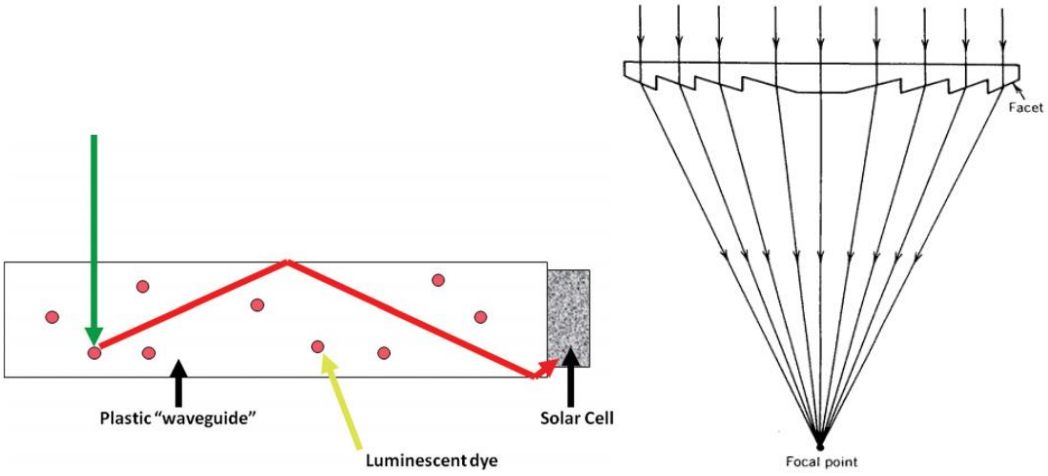

Figure 3: Principle operation of fluorescent solar concentrators [5] and lens-based solar concentrator [7].

In the design of a lens-based solar concentrator, the benefit of collection of sunlight from a large area and focus of the sunlight into a small area of a solar cell is provided. On the other hand, sunlight cannot be concentrated into the small solar panel as the sun moves naturally the whole day if the lens is fixed in one specific position. Hence, in lens-

based concentrators, solar panels have only a chance to get high intensity sunlight at one time through the day. With the addition of motorized tracking components to move the lens the expense must be taken into account, which restricts the applications as well.

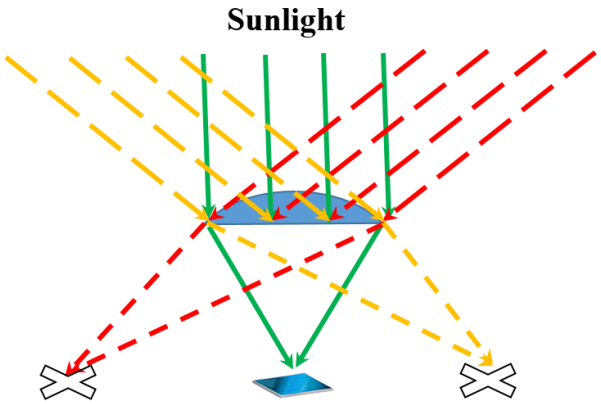

Figure 4: The low chance to absorb high intensity sunlight for the solar panel on the bottom with position-fixed lens in the solar concentrator.

1.2 Project Objective

For the Fluorescent Solar Concentrator (FSCs), if the transparent substrate (suitable polymer material) in which the luminescent particles are embedded can be thermally treated to move, so as to transport the particles inside it following the shift of the hot source in this project, the higher sunlight intensity can be absorbed more efficiently if this transportation is applied into an actual Fluorescent Solar Concentrator, achieving the goal of the movement of the luminescent particles following the sun.

For the lens-based solar concentrator, the lens should be formed at selective areas along with the movement of the sun, functioning as a "moving" lens, to be located appropriately under the shining of the sun all the daytime, for focusing a maximum of sunlight on specific points of the solar panel at the bottom of the solar concentrator.

1.3 Theory

1.3.1 Surface Tension

As an alternative to motorized mechanical lens movement, we examine polymer lens materials that offer the opportunity to modify their shape and hence the location of their focus.

Based on the development of thermal properties, various regular low-cost polymers can be adopted for the two modified material devices, and surface tension has acted as a central role in the polymer-based application.

In the pure liquid, all the molecules inside the bulk are attracted with an equal force by the neighbouring liquid molecules, resulting in a zero net force in all directions. However, molecules located at the liquid surface are not within the same situation comparing with the molecules inside the liquid, which do not have the molecules nearby to provide a balanced attraction force. Instead of forming a flat surface, surface molecules are pulled inward with the result of force difference by the neighboring molecules as shown in Figure 5 [8], developing an internal pressure. As a result, the liquid surface automatically contracts its area to maintain the lowest surface free energy. For example, the shape of small droplets and bubbles are spherical or nearly spherical in daily life, which gains the minimum surface area for a certain volume. This intermolecular force to minimize surface area is defined as the surface tension.

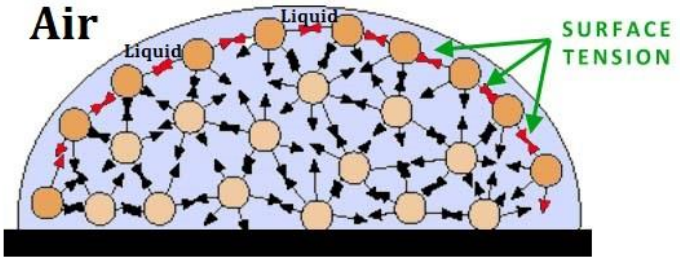

Figure 5: Surface tension is caused by the unbalanced net force of the neighbouring molecules at the liquid surface.

Surface tension is dependent on the temperature: the surface tension decreases with the increase of temperature, reaching zero at the critical temperature. Lorand Eötvös phenomenologically found and published the Eötvös rule in 1886 [9].

$$\gamma V^{2/3} = k(T_c - T)$$

Equation 1: the Eötvös rule [10].

Here, V is the molar volume of a substance. T_c is the critical temperature, γ is the surface tension and k is a constant valid for almost all liquid. A typical value of k (the Eötvös constant) is 2.1×10^{-7} $(J\cdot K^{-1}\cdot mol^{-2/3})$. For example, $V(18ml/mol)$ and $T_c(374℃)$ can be used for water.

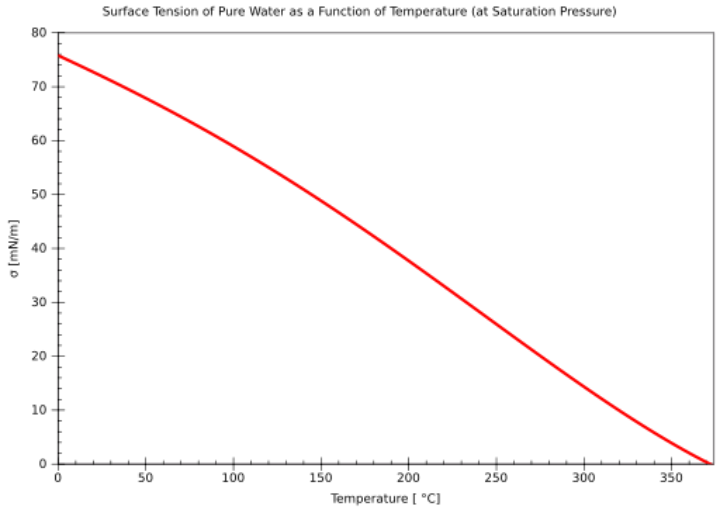

Figure 6: Surface tension of pure water as a function of temperature (at saturation vapor pressure: The evaporation in a closed container will discontinue until there are as many molecules returning to the liquid as there are escaping into the container above the liquid. At this point the vapor is saturated, and the pressure of that vapor is the saturated vapor pressure) [11].

At lower temperature, 6 kelvins as the temperature offset is provided for the formula with a better fit to reality, which is an improved version on Eötvös described by William Ramsay and Shields in 1893.

$$\gamma V^{2/3} = k(T_c - 6K - T)$$

Equation2: A variant on Eötvös is described by Ramsay and Shields [12].

However, this is still only an empirical equation to relate surface tension and temperature.

Applying this temperature dependent surface tension property of a molten polymer to low-cost and optically transparent polymers in this research, the idea of expanding their application for solar energy tracking and light concentrating can be realized through two different types of device design. Since this relationship between surface tension and temperature change is a common phenomenon for all kinds of liquids, several trials of

polymers are conducted for explanation and comparison of optimizing the experimental conditions to ensure a better result with higher light intensity and opportunity for practical utility.

1.3.2 Rayleigh-Bénard Convection

As a polymer layer is subjected to localized heat from below (See Figure 7) the increase in temperature of the bottom plane breaks the equilibrium of the liquid, causing the temperature to no longer be the same in all parts of the liquid. Before the heat is applied, the liquid temperature is precisely uniform: it can be observed to be the same at any position, and it has the ability to go back to its uniform state after one local, temporary perturbation. With the slight temperature increase of the bottom layer, a flow of thermal energy is conducted through the liquid. The temperature and the density will vary between the bottom and top plane. A uniform linear temperature gradient will be established. Buoyancy, and hence gravity will act as a driving force for the initial movement of the upwelling of lesser density fluid from the heated bottom layer of liquid [13]. In order to preserve a horizontal (or nearly horizontal) liquid surface, cooler surface liquid with higher density will descend, which forms the Rayleigh-Bénard convection process as shown in Figure 7. It is one of the most commonly studied phenomena because it can be obtained by a simple experiment first explored in detail by Henri Bénard, a French physicist, in 1900 [14].

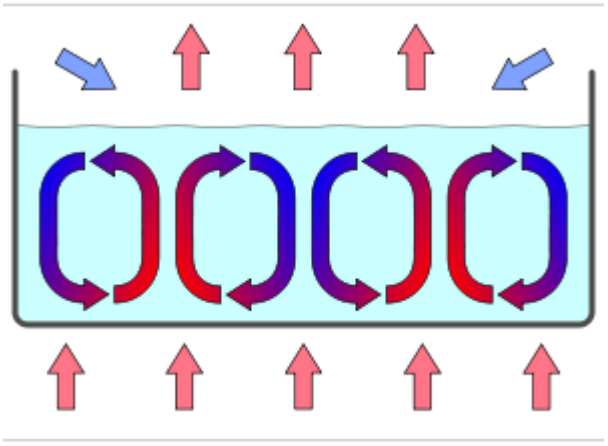

Figure 7: Rayleigh-Bénard convection in a gravity field.

In this thesis, melted polymer in a liquid state with a spatially applied thermal gradient will form a surface distortion, which is expected to be operated as a lens for optical purposes.

1.3.3 Bénard-Marangoni Flow Effect

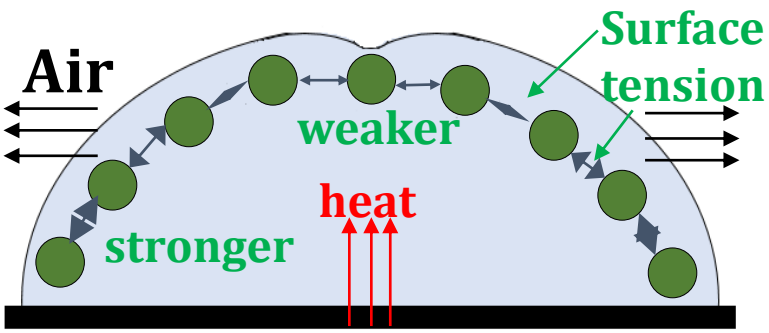

Figure 8: Schematic of Bénard-Marangoni flow effect.

When a surface tension gradient exists due to a thermal gradient at the surface of a liquid polymer, the liquid polymer with a higher surface tension pulls more strongly on the surrounding liquid than the liquid with a lower surface tension, and a mass flow will be initiated: the liquid will flow away from the region of low surface tension. This phenomenon is called Bénard-Marangoni flow effect [15], a general effect named after

Italian physicist Carlo Marangoni, who studied it at the University of Pavia and published his results in 1865. In addition, Bénard's research essentially consisted of observing cellular convection in pools and noting that upwelling of hot liquid occurred below centers of depression of the surface of a pool. Bénard attributed this anomaly to surface tension effects [16].

As shown in Figure 9 below [17], the interfacial tension of an interface is generated weakened when some molecules are located on to an interface between two phases (for example, oil and water). Especially, molecules that strongly absorb on interfaces are called surfactant. The surface tension gradient between surfactant (with both oil-friendly part and water-friendly part) and water will flow the oil phase (inhomogeneity) away from water, for cleaning purpose.

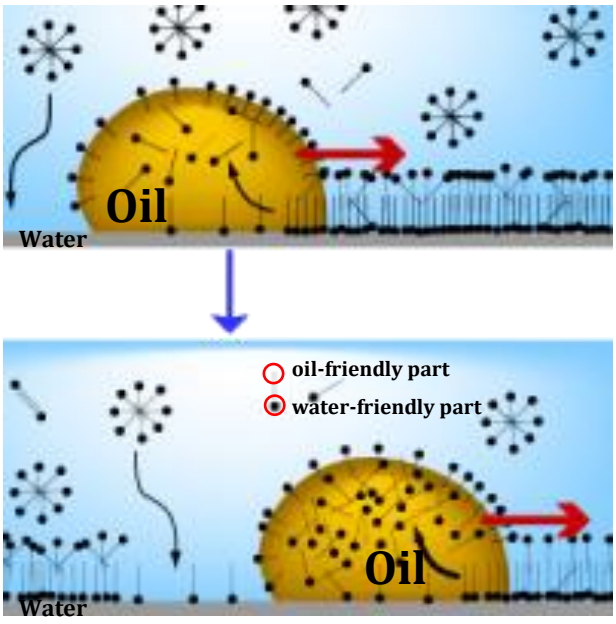

Figure 9: Bénard-Marangoni flow effect in surfactant application [17].

Applying this flow effect we can also understand a method for drying silicon wafers after a wet processing step during the manufacture of integrated circuits. After the wet processing, liquid droplets left on the surface of the wafer will cause oxidation that damages components on the wafer. To prevent damage from droplets, an alcohol vapor or other organic compound in gas or vapor with low surface tension is blown through a nozzle over the wet wafer surface, and subsequently a surface tension gradient caused by the flow effect in the liquid promotes the organic compound to pull the liquid blots easily and completely off the wafer surface to the deionized water bath, ensuring a dry wafer surface effectively. With low viscosity and fast evaporation rate, the organic compound will evaporate completely.

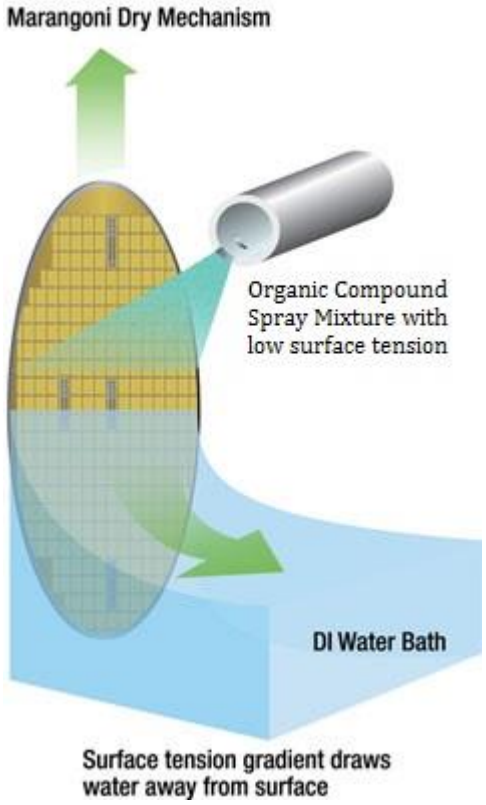

Figure 10: Surface tension gradient draws water away from surface [18].

As surface tension is observed as a function of temperature, the Marangoni flows can be induced by temperature gradient as well. Considering a horizontal fluid layer heated from below (as shown in Figure 11 [19]), the warmer fluid with lower surface tension will be pulled away from the hot area to the cold area. Combining with Rayleigh-Bénard convection, the flow and convection phenomenon will be obtained at the same time.

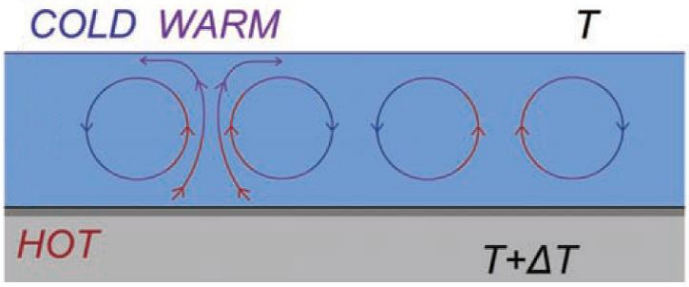

Figure 11: Thermal convection in a plane layer [19].

For this project, the combining concepts of both Rayleigh-Bénard convection and Bénard-Marangoni flow effect are applied to selected polymers so that selected luminescent particles can be transported efficiently and light can be concentrated by an expected formable polymer lens for different applications of solar utility as mentioned above. Both of them will essentially improve humans' ability of exploiting solar energy more efficiently in the event that these material devices can be integrated into a concentrating fluorescent solar collector.

1.4 Material Selection

1.4.1 Movement of Luminescent Particles

There are two types of results in this thesis. For the first type – movement of luminescent particles on melted polymer for FSCs optimization, the two major components, luminescent particles and polymer, need to be taken into account.

In one typical FSCs design, the re-absorption of the emitted light by an adjacent luminescent dye is one of the main losses which contribute to their low efficiencies. In order to overcome this loss, the luminescent dye can be situated within specific locations to avoid the re-absorption of the emitted light from the adjacent dye and with a convex lens on top of it to ensure a higher intensity sunlight can be concentrating to the dye at each specific site. However, because of the movement of the sun all the daytime and the position of luminescent dye is fixed, the high intensity sunlight can only be concentrating to the dye one time when the sun is right on the top of the dye.

In this first result, the luminescent dyes have the ability to follow the movement of the sun without losing sunlight when the sun is not directly above the FSCs, which is realized by the movement of select polymers when thermally treated. The intensity of light absorbed by the luminescent particles can be enhanced.

1.4.1.1 Selected Polymer (Crystal Bond and Hot Melt Glue Stick)

With respect to the support of luminescent particles and optical transmission requirement, the low-cost and low-melting point polymer with the ability of being optical transparent when melted is selected for the transportation of luminescent particles. Two

kinds of polymers evaluated for comparison are: Crystal Bond 508 Ultra Amber and Hot Melt Glue Stick from Benchmark.

In order to decide on the appropriate polymer substrate, melt viscosity, a temperature-dependent property, showing lower viscosity at higher temperature, must ensure a fluid state for the polymer above the melting point to transport the luminescent particles. Because both types of polymer are commercially used as melting adhesives the property of low viscosity can be expected.

Both crystal bond and hot melt glue stick are measured with differential scanning calorimetry (DSC) for melting point as shown in Figure 10.

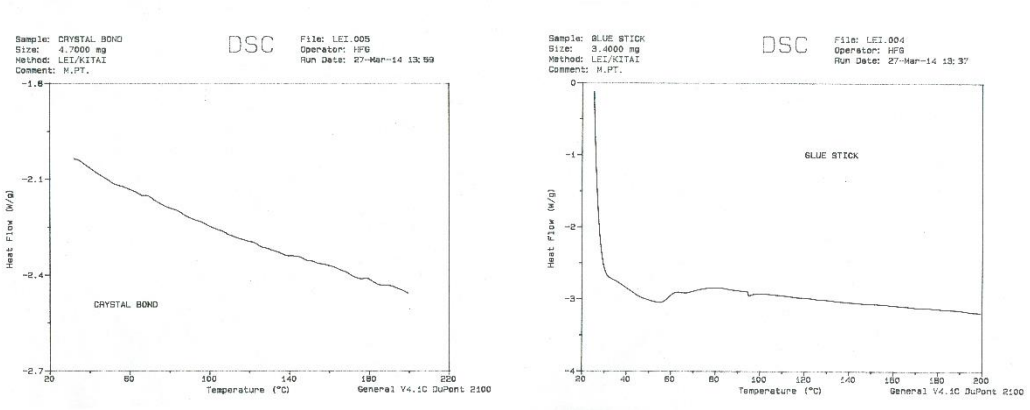

Figure 12: DSC Analysis for Crystal Bond and Hot Melt Glue Stick.

From the results of DSC analysis, the thermal transitions of polymeric materials are determined, which are observed for comparing materials. Melting points and glass transition temperatures for most polymers can be measured from this standard compilations. Melting point (T_m) depends on the molecular weight of the polymer, hence lower molecular weight may have a lower melting point than expected [20].

From the DSC curve of two kinds of polymers shown in Figure 12 above, the slope of the curve represents heat capacity. The obvious slope difference is representing various heat capacity before and after 30 ℃, meaning a significant phase change at that temperature, which is compared with no phase change observed from Crystal Bond's curve. The sharp change is caused by a different thermal property with high temperature, which allows for different ability to move the luminescent particles.

1.4.1.2 Luminescent Particle (YAG:Ce)

Currently, YAG:Ce is widely adopted in light emitting diodes (LEDs) to generate yellow light from the blue light generated by indium gallium nitride, then the bright white light will be produced with the combination of the emitted yellow light with the non-converted blue light [21]. As shown in Figure 13, the theoretical excitation and emission profile at the peaks of 450 nm and 550 nm are observed, separately. Despite the fact that there is a region that light is not absorbed at all in the excitation spectrum, these luminescent materials can exploit a suitable portion of the wavelength range up to 550 nm.

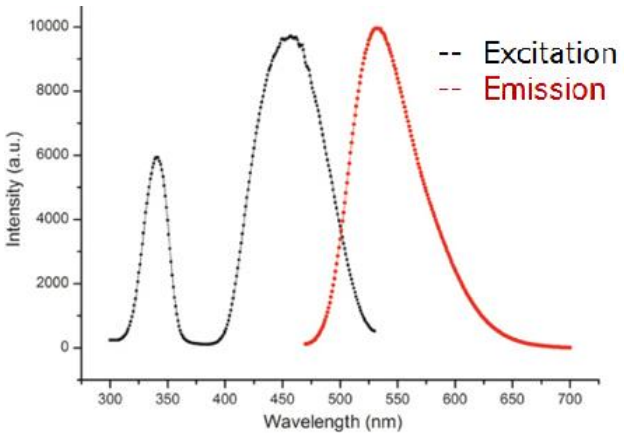

Figure 13: Theoretical excitation and emission spectra of YAG:Ce [22].

The application of YAG:Ce in light emitting diodes (LEDs) has a requirement of ability of being highly stable and maintaining its quantum efficiency at high temperature. Figure 14 shows that the quantum yield of YAG:Ce remains relatively high even under elevated temperature [23]. This behaviour is a confirmation of its stability when subjected to a large amount of energy (i.e., with localized heat or under sunlight concentration effect). And the ability of avoiding degradation when these materials are exposed under sunlight is also required.

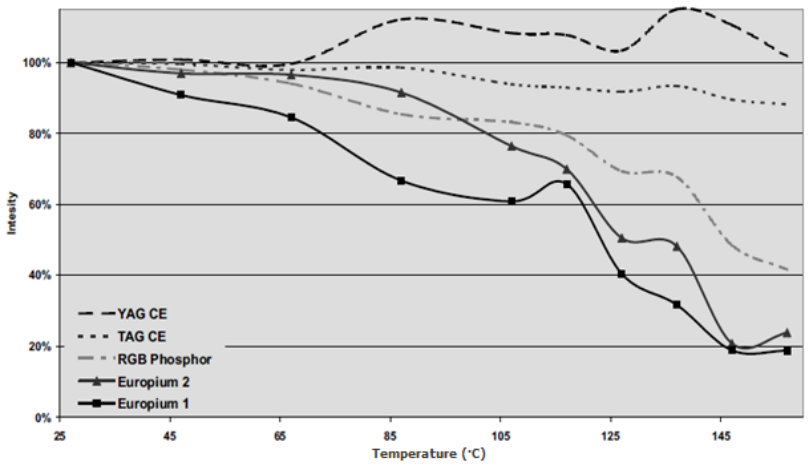

Figure 14: Phosphor's luminescence vs. temperature [23].

1.4.2 Polymer-based Deformable Lens

For the second type – polymer-based deformable lens for solar tracking, there is one main component, a suitable type of polymer to form expected lens, needs to be considered.

1.4.2.1 Selected polymer (polystyrene)

To produce an optical lens with thermal treated polymer, the following properties must be provided: transparency to light, suitable operating temperature (low softening

point) and non-toxic to the environment. Polystyrene is well qualified to satisfy the demand of actual solar concentrator device application.

Polystyrene (PS) is a synthetic polymer made from the monomer styrene as shown in Figure 13. The expense of this kind of polystyrene per unit weight is low (~ 4 cents per pound) [24], and the scale of its production is several billion kilogram per year [25]. Polystyrene is naturally transparent with relatively low melting point [26].

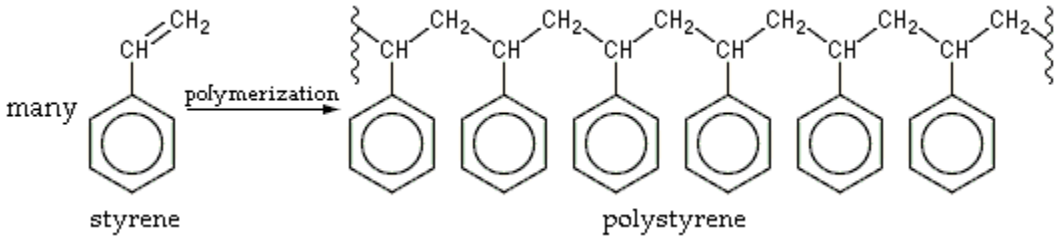

Figure 15: Polystyrene obtained through polymerization of monomer styrene.

In physical terms, as a thermoplastic polymer, polystyrene is solid at room temperature but flows when heated above around 100 ℃, which is its glass transition temperature. It will become rigid again when cooled down.

In chemical terms, with a formula of $(C_8H_8)_n$, polystyrene is a long chain hydrocarbon in which carbon centres are attached to the aromatic ring benzene. The material's properties are determined by the molecular chains existing in the irregular confirmation. Thus polystyrene is amorphous with atactic chains. Since it does not contain crystals to scatter the light, polystyrene is also transparent.

For better study and explanation of the functioning of this polymer-based lens, the mathematic equation of lenses is adopted approximately ignoring optical effects due to the thickness of lenses to simplify ray tracing calculations.

1.5 Basic Optics and Lens Equation

In optics, the thickness of a thin lens (distance along the optical axis between the two surfaces of the lens) is negligible compared to the radius of curvature of the lens surface.

The focal length for a thin lens in air is the distance from the center of the lens to the focal points of the lens, which is positive for converging lens (a light beam with parallel light will be focused to a single spot after passing through the lens) and negative for a diverging lens (a light beam with parallel light will be diverging after passing through the lens) as shown in Figure 16.

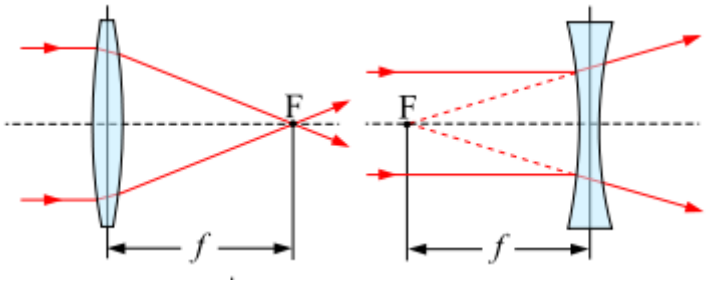

Figure 16: The focal point F and focal length f of a converging lens (for example a convex lens) and a diverging lens (for example a concave lens).

For a spherically curved mirror in air, the focal length is equal to the radius of curvature of the mirror divided by two, which is $f = \frac{R}{2}$ (R is the radius of curvature of the mirror's surface).

There is a relationship between the object distance (o), image distance (i) and focal length (f) as shown below, in which the object distance (o) is the distance between the light source and the lens and the image distance is the distance between the lens and the screen [27].

$$\frac{1}{o} + \frac{1}{i} = \frac{1}{f}$$

$$\frac{1}{\text{object distance}} + \frac{1}{\text{image distance}} = \frac{1}{\text{focal length}}$$

Figure 17: Thin Lens Equation.

1.6 Method of Thermal Modelling

Depositing selected kinds of polymer sample on the top surface of temperature-controllable heat source was the start-up of the second type of research. According to the temperature profile of the heat source dependent thermal property of the polymer sample, and for better comparison between the theoretical and experimental results, COMSOL Multiphysics was applied to model the temperature distribution on the surface of the heat sources having various sizes and different heating powers.

COMSOL Multiphysics is a finite element analysis and simulation software package for various physics and engineering applications. With an installed heat transfer module, the mechanisms of heat transfer-conduction, convection and radiation can be studied with simulation tools.

In this modelling, the boundary conditions, geometry of the heat source, materials of the heat source and ambient, and heat transfer coefficient differing from on the top surface to on the bottom surface can be assigned to the model, and top surface temperature profile of the heat source is exhibited in both direct cross-section view and 1D plot in Temperature vs. Position.

The geometry of polymer-based lens forming from the change of thermal properties is highly depending on the temperature profile, hence the more precisely the theoretical

results are obtained from the COMSOL Multiphysics heat transfer modelling, the better explanation and study of the inducing mechanism of lens formation can be realized .

Chapter 2: Experimental Procedure and Analysis

Because this thesis consists of two projects, the experimental procedure and analysis approach will be shown in detail separately. In the following, section 2.1 and 2.2 are about the design and analysis approach for the movement of YAG:Ce on melted polymer and the section 2.3 and 2.4 are about the design and analysis approach for the polymer-based deformable lens.

2.1 Design Concept for The Movement of YAG:Ce on Melted Polymer

2.1.1 Polymer Pre-Treated and YAG:Ce Deposition

Crystal Bond 509 amber and Hot Melt Glue Stick from Benchmark were melted separately at the top surface of a microscope cover glass ($22mm \times 22mm$) from VWR International company, locating on the top of a temperature controllable hot plate for 15 minutes to ensure a nearly flat polymer surface without bubbles. A thin, uniform polymer layer with a thickness of 0.1 mm was obtained.

The microscope cover glass with a thickness of 0.15 mm was chosen because of the ability of thin glass to prevent excessive heat dissipation during the operation of the thermal experiment and to withstand high temperature without melting or any related deformation. This type of glass can support the melted polymer sample and be transparent for light transmission.

Figure 18: Microscope glass cover.

After 30 minutes to allow for the melted polymer layer to cool down, luminescent particles comprising of single crystal YAG:Ce with Ce doping level of 0.180 at.% at an average particle diameter of 4 ~ 8 μm obtained from Phosphor Technology Ltd., was spreading in a line on the top side of the polymer layer. YAG:Ce particles with light weight can be supported and keep stable on the specific position.

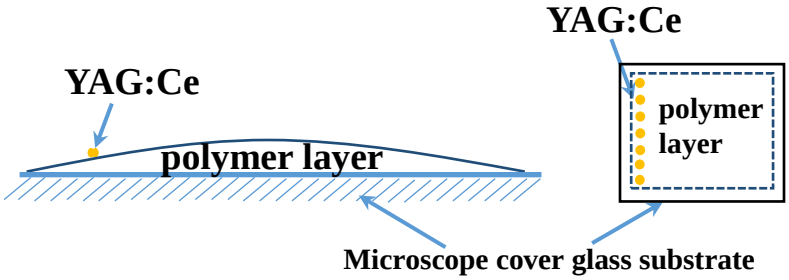

Figure 19: Schematic of Cross-section and top view of YAG:Ce at the top surface of polymer on the microscope cover glass substrate.

The sample was then installed under a wire heater equipped with a motorized slider as described in detail below.

2.1.2 Experimental ApparatusSetup

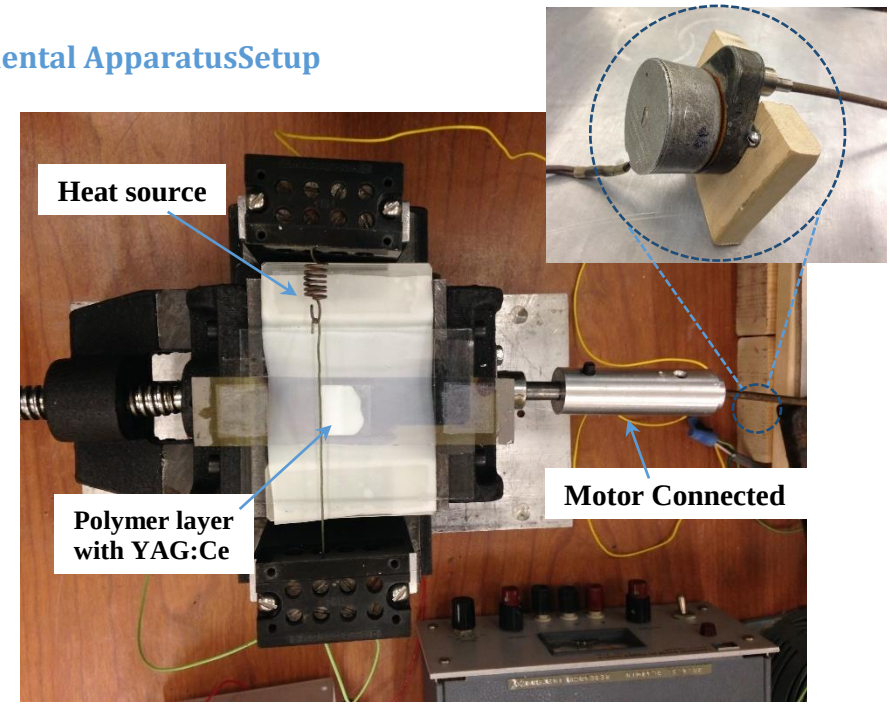

Figure 20: Top view of experimental setup.

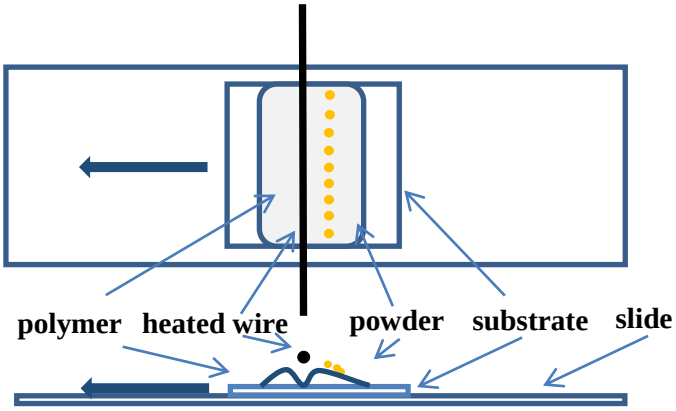

Figure 21: Schematic of the experimental setup.

The experimental apparatus was modified from a standard machine slide as shown in Figure 20, by adding a straight chromel wire (made of approximately 90% nickel and 10% chromium [28]) as heating source when applied current to generate heat, The polymer layer with YAG:Ce on top of it was placed underneath, with the heating wire 0.5 mm away from the top surface of polymer sample, to prevent the hot wire touching and

burning the sample. The hot wire was fed by a DC power supply, which can be controlled with a knob at a range of 0 ~ 15 V. Because low melting point polymers were employed, approximately 3 V was supplied for this experiment.

The system was motorized with a low velocity motor connecting at the end to pull the slide of 4 μm per second, at which speed the melting and cooling process of polymer could hold enough time to be equilibrium state in order to move the "reacting" zone forward as if the zone followed the movement of heating source [29], hence the YAG:Ce could be transported successfully.

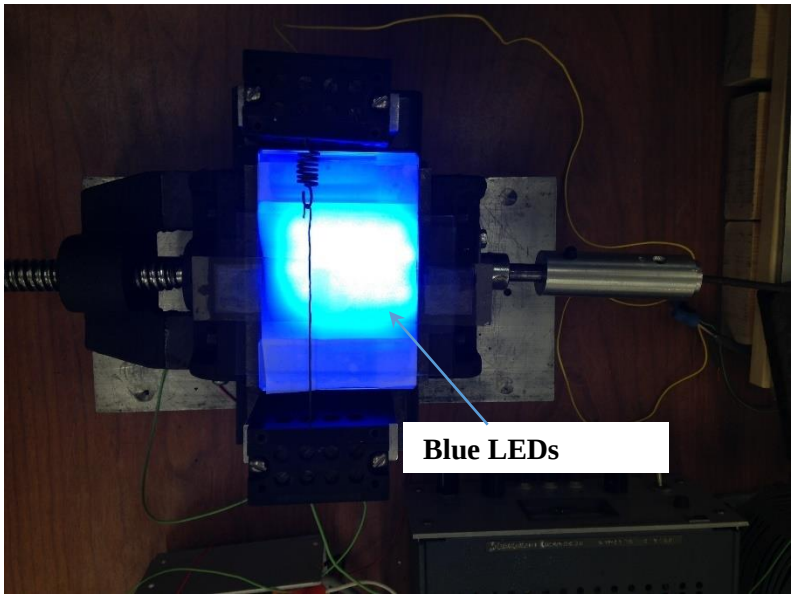

Figure 22: Blue LEDs shining from beneath the polymer sample.

For better observation of particles movement, a blue LEDs module was installed beneath the polymer sample, illuminating YAG:Ce particles when they were transported by the fluid polymer sample.

Since the selected polymer layer and supporting microscope cover glass are both transparent, blue light could travel through and excite the yellow luminescent particle more directly.

To determine experimental parameters and record the results more clearly, a number of instruments and tools have been adopted throughout the course of this research, including wetting angle measurement for the polymer sample after experiment, the polymer thermal expansion property and particle movement recording. The wetting angle measurement and results recording were operated based on the machine slide. These are described in detail below.

2.2Analysis Approach for The Movement of YAG:Ce on Melted Polymer

2.2.1 Laser-Based Wetting Angle Measurement

The ability of particle transport for each type of polymer sample depends on the polymer wetting angle (as shown in Figure 23).With a greater wetting angle, a larger pushing force could be issued for moving particles more efficiently by melted polymer.

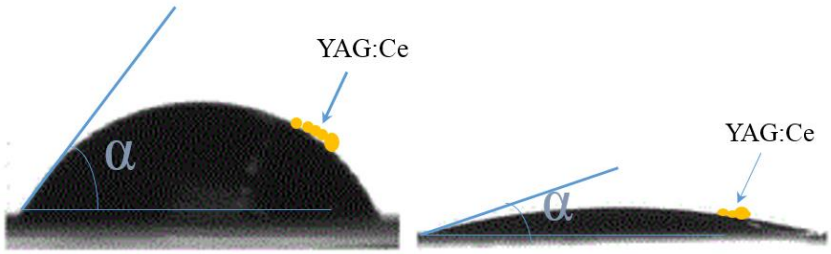

Figure 23: Different wetting angle forming by melted polymer.

A laser-based measuring method was developed to determine the wetting angle and view the surface profile of the melted polymer after cooling down the polymer or in-situ, which consisted of a single beam laser, a white axis screen and a high resolution Webcam.

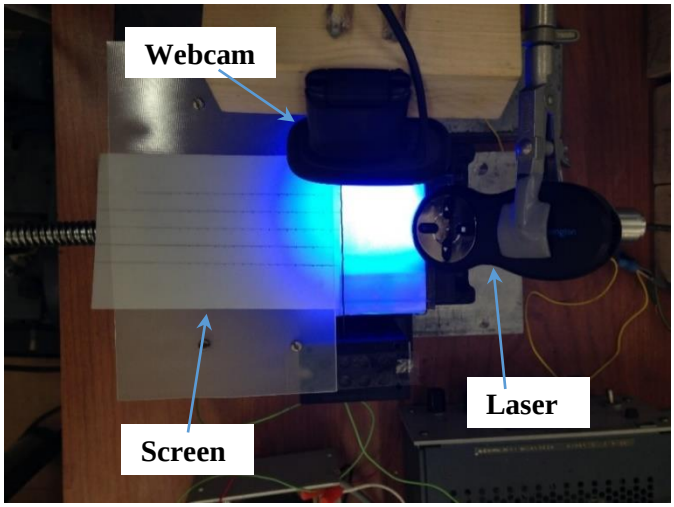

Figure 24: Laser-based wetting angle measuring method.

The working principle of this measuring method is shown in Figure 25. The single laser beam is incident at an angle (θ = 55 °) to the surface of polymer sample, and the reflected light will shine on the axis screen (placed on the top of polymer sample at a height of 1.8 cm) with a red laser dot (as shown in Figure 26). Using a Webcam to record the position of the laser dot, the angle α could be obtained with this method after measuring selected lengths and calculation at each 0.48 mm of sample movement (the speed of motor of 4 μm/s times the 2 minutes time interval image capture). By this method it was possible to gather all the angles at different positions to obtain the surface profiles and thus the wetting angle in a cross section view. The detailed calculation of α is explained in Figure 25:

- Measure the distance L' between a and the laser dot
- Calculate β with the equation: $\beta = \arctan(\frac{L'}{H})$
- Obtain γ with the equation: $2\gamma = \theta + \beta$
- Get the angle α with the equation: $\alpha = \theta - \gamma$

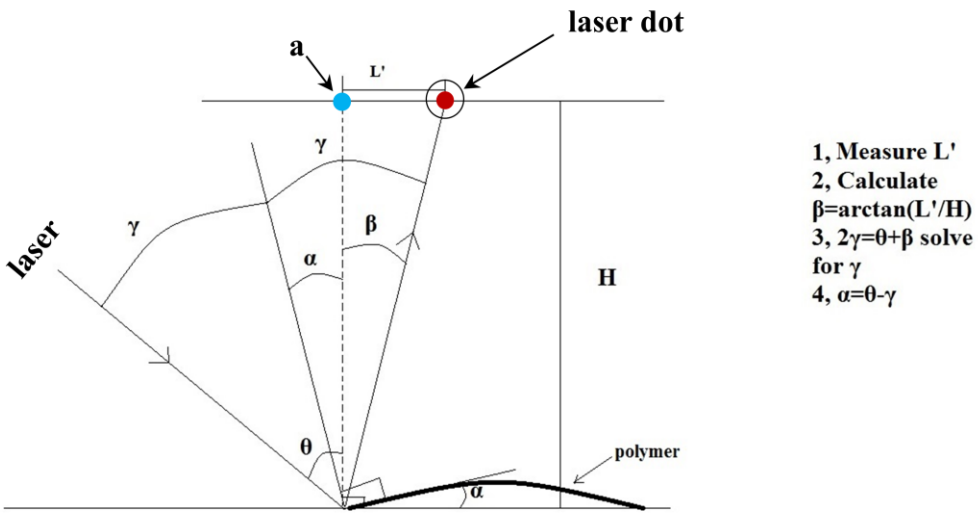

Figure 25: Working principle of the wetting angle measuring method.

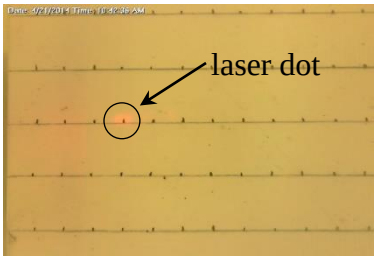

Figure 26: The red laser dot shining by reflected laser light.

Also with the same Webcam installed on the right top of the melted polymer sample without the laser and the axis screen, the whole YAG:Ce particles transport process was recorded with a time-lapse photography software with 2 minutes time interval image capture. With assistance of this photography software, the Webcam was able to take pictures after each 2 minutes. Because the speed of the motor connected to the slide as mentioned before was too gradual to be observed within a short time and one whole transportation process would take around 2 hours, 60 pictures could be taken for better observation and analysis, and reviewed rapidly to create a time-lapse movie of the process.

Besides information given from the pictures, the clear recording video file ensured a straightforward result to understand the way of particle movement and change of the polymer sample when the melting part was located beneath the hot source and the cooling part was away from. Accurate information can be accessed with a time label on the left top of the recording video footage, comparing with the wetting angle of melt polymer sample measuring at different moment.

This type of research is highly depending on the thermal behaviour of the selected polymer sample, the thermal expansion and weight loss of hot melt glue stick at different temperature were measured for understanding the polymer transportation behaviour.

2.2.2 Thermal Expansion and Weight Loss Measurement

With a measuring cylinder containing solid hot melt glue stick at room temperature, the thermal expansion of this polymer at different temperature can be measured in an isothermal equipment – FISHER Isotemp® Oven SENIOR MODEL.

By adjusting the temperature (range of 25 ~ 195 ℃) of the isothermal oven, reading the volume of polymer after each 15 minutes to make sure the equilibrium state can be reached at each temperature, the volume vs. temperature curve of hot melt glue stick can be plotted, combing with the experiment record, the research can be explained with a more in-depth understanding.

The weight-loss of hot melt glue stick was measured with temperature adjustable and readable hot plate and an accurate balance with readability of 0.001 g. Starting from room temperature, the weight of the polymer was recording at 10 degree intervals after each 15 minutes.

Both types of data collected from the measurements above are applied with the surface profile obtained from the laser-based measuring method. Because the wetting angle is the major cause for particles movement, the angle forming mechanism when the polymer sample was heated are required to be studied with the information obtained through the measurement introduced above.

2.3 Design Concept for The Polymer-based Deformable Lens

Another kind of heating source, representing the sunlight, with predictable temperature profile and controllable width was prepared for the second type of research. The chosen low melting point and low cost polymer sample was deposited on the top surface of the heating source, instead of the surface of microscope cover glass. Then the prepared sample was placed in a glass-sealed chamber with the protection of N_2 atmosphere.

2.3.1 Patterned ITO (Indium Tin Oxide) Heating Source Preparation

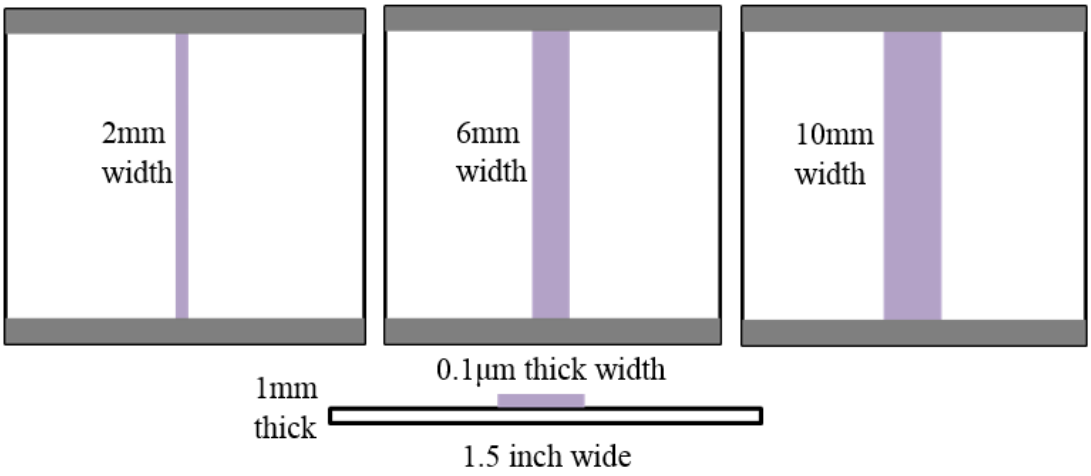

Figure 27: Dimensions of the ITO coated glass heating source.

The ITO (Indium tin oxide) heating source was prepared based on a thin ITO layer with a thickness of 0.1 μm, coated on one side of a Corning® 1737 glass substrate having a thickness of 1 mm. ITO is a widely used transparent conducting oxide with two chief properties: the electrical conductivity and optical transparency. It is a heavily-doped n-type semiconductor with a bandgap of around 4 eV [30]. With this large bandgap, ITO is mostly transparent in the visible part of the spectrum.

By changing the width of ITO stripe, the temperature profile of this patterned ITO heating source can be controlled. The ITO heating source preparation process is shown in Figure 28. Starting with rinsing one piece (1.5"×1.5") ITO coated glass with deionized water and drying the glass in flowing dry N_2, and two digital hot plates with temperature at 110 ℃ and 130 ℃ respectively, the ITO coated glass was spin-coated with Shipley positive photoresist S1808 with the spin-coater (Headway Research Inc., Model EC101) to the surface of ITO for 30 seconds with 1000 rpm in the following steps:

- Load Corning® 1737 glass onto the center part of the vacuum chuck
- Switch on the vacuum connected to the coater and hold to secure the glass
- Apply 30 drops of SOG solution uniformly on the surface of ITO side with clean pipet
- Set the parameter of the coater with spinning speed and spinning time and start spin-coating
- After 30 seconds, spin-coater stops automatically, switch off the vacuum to release the glass

Then the coated glass was soft-baked at 110 ℃ for 2 minutes. A thin nickel mask with a stripe (width of 2 mm, 6 mm, 10 mm, individually) was placed intimately against the coated glass using magnetic force. After the whole mask-covered glass with a layer of photoresist was exposed with UV light (350 ~ 450 nm) for 30 seconds, the exposed photoresist was immersed into developer bath for 40 seconds with gently shake the bath for the better dissolution of the exposed photoresist. Then the glass was rinsed thoroughly with deionized water and blow dry with N_2 [31].

The ITO coated glass was moving into HCl (Hydrochloric acid, 36.5 ~ 38%, CALEDON Laboratory Chemicals) for 15 minutes in order to etch away the exposed ITO coating. After that, the remaining photoresist on the glass was dissolved into acetone. Then the glass was rinsed thoroughly with deionized water and blow dry with N_2. The ITO coated glasses with patterned stripe of different width were obtained [32].

For better electrical conductivity, both ends of the ITO stripe was electroplated with nickel thin film. One end of the ITO stripe was placed into the nickel plating solution (Easyplate Nickel plating solution #C-2, Dalmar Manufacturing Co.) onto a digital hot plate at 90 ℃ with the magnetic stir bar with a rotating speed of 150 rpm. The other end was connected to the Cathode of HP6217A power supply at 3 V. A nickel strip was placed into the plating solution and connected to the anode. The electroplating time is 5 minutes, and the same process was finished for the other end [33]. Then the ITO coated glass heating sources with the width of 2 mm, 6 mm and 10 mm were obtained as shown in Figure 27 and 29.

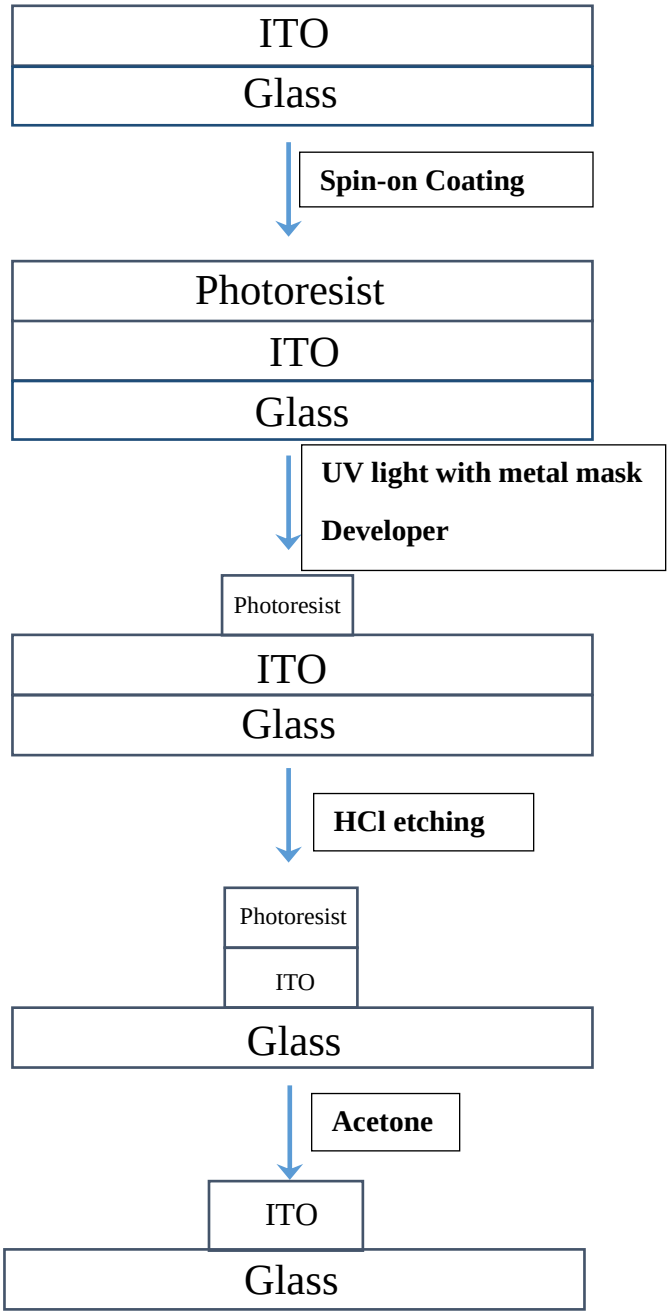

Figure 28: Schematic of ITO heating source preparation process.

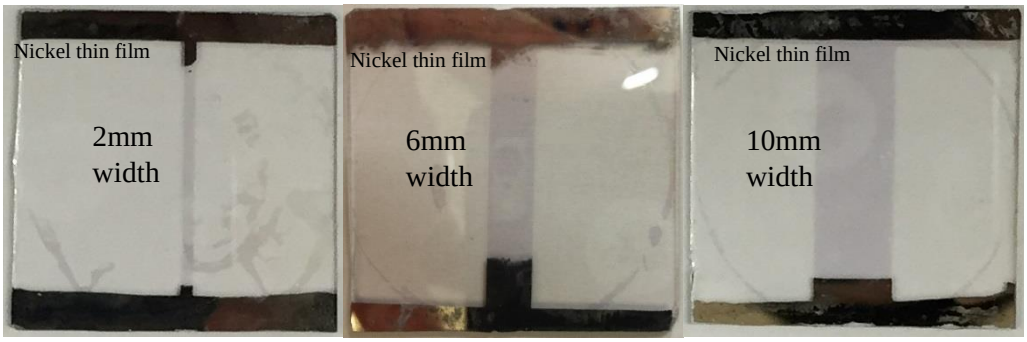

Figure 29: Top view of the ITO coated glass heating source.

2.3.2 Polymer Dissolving and Casting on The Surface of ITO Coated Glass

For the second project in this thesis, the polymer-based thermally generated lens, polystyrene with average molecular weight (M_w) of 35,000 in the format of beads was purchased from *Sigma-Aldrich*® Corporation. Its density is 1.06g/ml at 25 ℃ with a glass transition temperature of 123 ~ 128 ℃ [34].

Figure 30: Polystyrene beads from *SIGMA-ALDRICH*®.

Three kinds of organic solvent (toluene, tetrahydrofuran and chloroform) [35] were adopted for dissolving polystyrene beads, casting a uniform polymer layer on the surface of ITO coated glass heating source and the purpose of comparison experiments.

Table 1: Properties of three kinds of organic solvent [36].

Parameter/Material	Toluene	Tetrahydrofuran	Chloroform
Chemical Formula	C_7H_8	C_4H_8O	$CHCl_3$
Density(20 ℃)	0.87 g/cm^3	0.8892 g/cm^3	1.489 g/cm^3
Viscosity(20 ℃)	0.59 cP	0.48 cP	0.563 cP
Vapor pressure (20 ℃)	21 mmHg	132 mmHg	155.25 mmHg
Boiling point	111 ℃	66 ℃	61.15 ℃

Polystyrene beads were dissolved into the three kinds of organic solvent at the mass ratios of Polystyrene (1): Toluene (1.7), Polystyrene (1): Tetrahydrofuran (1.8), and Polystyrene (1): Chloroform (3.0) and at the same volume ratio of Polystyrene (1): Solvent (2.0) in the fume hood with stirring, shaking and kept for 1 day for totally dissolved to a uniform and clear solution in three small screw cap sealed glass bottle.

Also in the fume hood, 10 drops of each solution were cast with a clean pipet onto the surface of patterned ITO coated glass heating source, and ventilated for 18 hours till most of solvent evaporated and a uniform thin polymer layer with an average thickness of 0.2 mm was obtained for the further experiment.

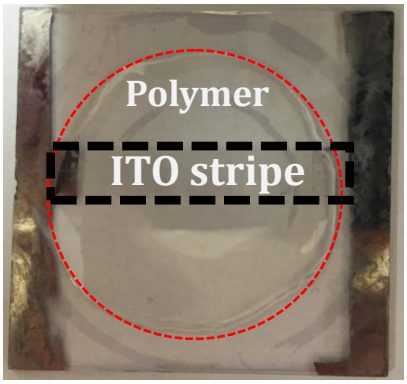

Figure 31: Top view of polymer layer on the surface of patterned ITO coated glass heating source.

2.3.3 Experimental Apparatus Setup

According to the properties of polymer, oxygen and oxidation must be avoided when the polymer is heat-treated. Hence, a sealed cabinet with N_2 atmosphere was employed.

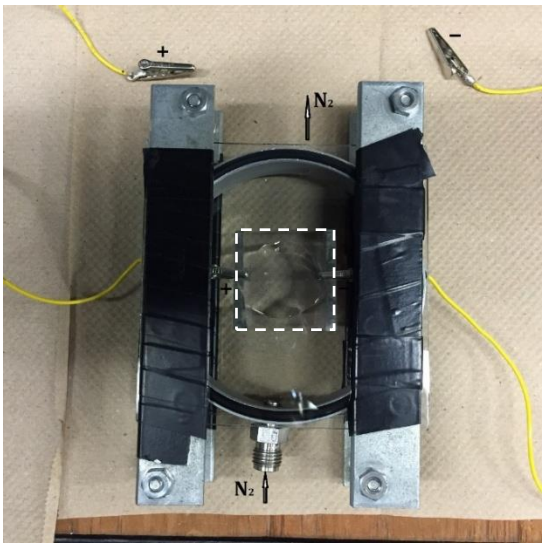

Figure 32: The glass sealed chamber with N_2 atmosphere inside.

The glass sealed chamber is applied to ensure N_2 atmosphere for protecting the heat-treated polymer from oxidation as shown in Figure 32. The chamber consists of two glass plates on the top and bottom with bolts and nuts clamps. There are two holes drilled

in the aluminium circle for N_2 flowing in and out. The patterned ITO coated glass sample with diluted polymer layer on the surface of it was located in the chamber in the direction as shown in Figure 31.

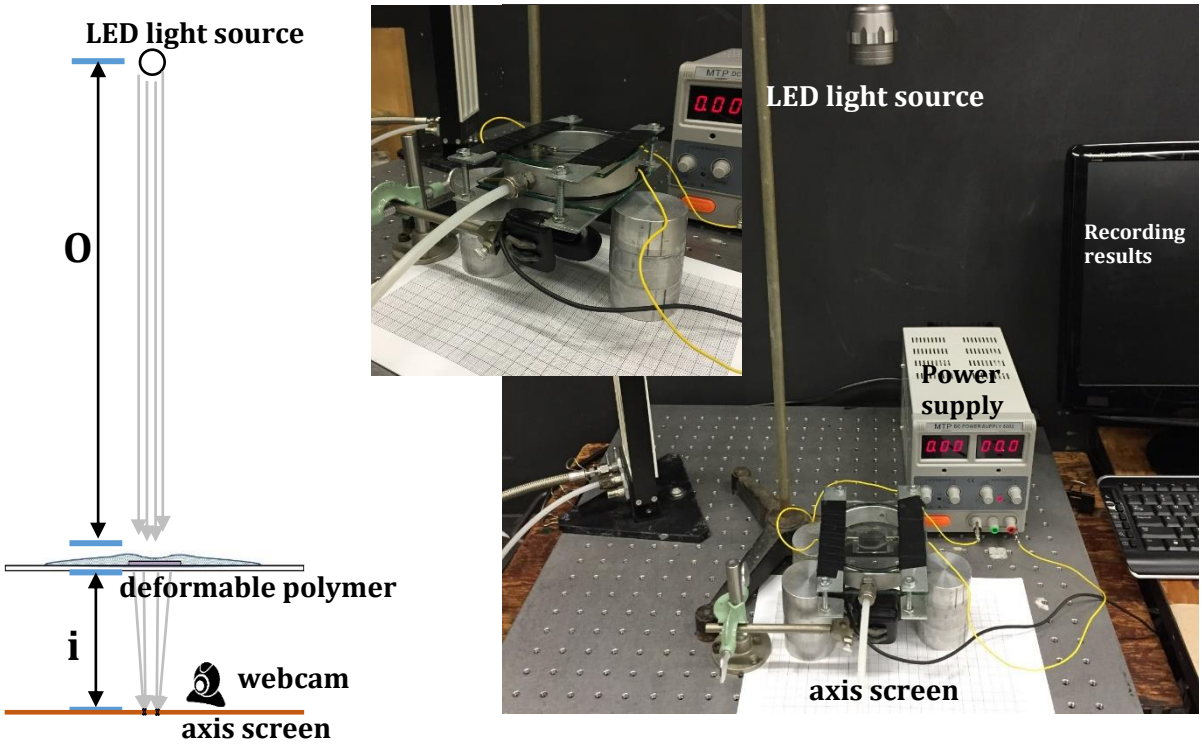

Figure 33: The experiment setup.

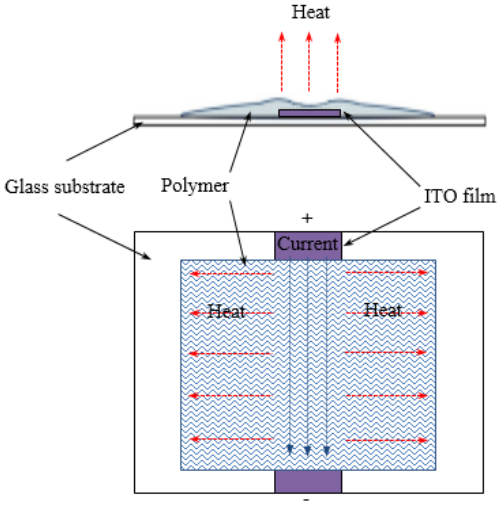

Figure 34: Schematic of the experiment setup.

As shown in Figure 33, the patterned ITO coated glass heating source inside the glass sealed chamber was connected with a current and voltage controllable digital display power supply to achieve the spatially defined heating. The power applied to the heating source is listed in Table 2 below.

Table 2: The Current and Voltage applied to the heating source with different ITO stripe width.

Width/Voltage	7 V	8 V	9 V
2 mm	0.06 A	0.20 A	0.30 A
6 mm	0.06 A	0.20 A	0.32 A
10 mm	0.06 A	0.22 A	0.35 A

The white light emitted from the top LED light source located at the object distance (o) of 44 cm, passed through the glass chamber and thermally deformable polymer lens, focusing on the axis screen, positioned at the image distance (i) to ensure the sharp line results. A webcam facing the axis paper was connected to a computer to record the focal properties.

2.4 Analysis Approach for The Polymer-based Deformable Lens

Several instruments and tools were applied for measuring the physical change of the ITO coated glass heating source and the dilute polymer layer during the process of experiment. For a better explanation of theory adopted to the formation of lenses, several trials were conducted as well. Combining with the clear record of focal results, a better understanding could be obtained. See below.

2.4.1 ITO Heating Source Surface Temperature Measurement

When the 2 mm, 6 mm and 10 mm width patterned ITO coated glass heating sources were applied with power, the surface temperature change was initiated. With a J-type thermocouple (Diameter 0.003", OMEGA Engineering Inc.), the surface temperature profiles of different ITO heating sources at various heating powers were measured. Because the ITO stripe width is at the scale of mm, this diameter and type of thermocouple ensured a precise reading at the selected region with higher sensitivity. Starting from the middle region of the ITO stripe, measurement was conducted at a division of 2 mm to the side with a bead-like small amount of silicone heat transfer compound (from M.G. Chemicals with high thermal conductivity of 0.657 W m^{-1} K^{-1} to enhance heat transfer between the thermocouple and the measuring surface for more precise temperature reading) at the end of the thermocouple, contacting the measured surface region of glass heating source. Then the temperature profile was plotted according to the position.

2.4.2 Polymer Layer Surface Profile Measurement

The surface profile of this thermally generated polymer lens was measured with CS-5000 formtracer from Mitutoyo Corporation. With this measuring equipment, the surface profile in the thickness of μm scale could be determined precisely. And the focal length of the polymer lens was also calculated through the surface profile for further optical study.

2.4.3 Light Concentrating Results and Image Distance (i) Determination

With a webcam facing the axis paper, the light concentrating results and the formation of sharp lines were clearly recorded as pictures and 2 minutes videos, individually. With assistant from the photometer, the image distance (i: the distance between the lens and the screen) could be determined by adjusting the position of axis paper and reading the highest luminance of the sharp lines. According to the thin film equation, the theoretical image distance will be calculated with the known object distance and focal length reading. A good comparison between the theoretical reading and the actual position of axis screen in the experiment could be obtained.

2.4.4 Weight Loss and Thermal Cycle Repeatability of Polymer Layer

Because of the high evaporation rate of organic solvent applied for dissolving the polymer beads in the research, polymer weights of different solution after various time length were measured.

The mass of polymers from the solution with toluene, tetrahydrofuran and chloroform organic solvents were weighed at different temperature with a temperature controllable hot plate for 15 minutes at each temperature to determine the heating temperature at which organic solvent in the polymer could cease vaporizing and the percentage could be stable.

And the three types of polymer layer were also measured the mass before and after 18 hours ventilating at room temperature to observe the weight difference between the solution casting on the surface of the heating source and the polymer layer for the thermal-treated experiment. Combining with the observation from the temperature

determined from the previous measurement, the starting percentage of the organic solvent in the polymer sample could be obtained from the polymer layer heated at the specific temperature for 15 minutes after 18 hours ventilating.

The masses of polymers from the solution with tetrahydrofuran and chloroform organic solvents were weighed before and after the thermal-treated at different heating power by the various ITO stripe width coated glass heating source.

The weight losses of the polymer sample from the solution with tetrahydrofuran organic solvents were measured within 5 days with one reading per day to observe the slight vaporization of the organic solvent in the polymer sample. After 5 days, all these polymer samples were heating at 100 ℃ for 15 minutes to release the remaining unstable organic solvent.

The thermal cycle repeatability of the polymer-based lens is required for the purpose of actual application in the industry. Heating the polymer sample after the thermal-treated experiment by ITO coated glass heating source at 150 ℃ for 15 minutes with a hot plate, the ability of cycle repeatability of the polymer sample was depending on whether the lens could be formed or not after the second time thermal-treated experiment by the heating source.

2.4.5 Reversing ITO Heating Source with The Polymer Layer on The Bottom

When the polymer-based lens formation was initiated and simultaneously concentrating light in the glass sealed chamber applied, the ITO coated glass was located approximately and not precisely at a horizontal position. To determine the effect of the heating source position on the focal properties the major role of two formation theories

(Rayleigh-Bénard convection and Bénard-Marangoni flow effect) which influenced the formation of the lens more significantly was invoked.

The experiment with the polymer layer on the bottom of the heating source was conducted in which the ITO coated glass heating source with diluted polymer layer on the top surface was reversed to be upside down with polymer layer on the bottom, to observe the effect on focal results compared to that from the normal position of the ITO heating source.

Chapter 3: Results and Discussion

As both projects are focusing on the more efficient utility of light by a) transportation of luminescent particles in the first research and b) concentrating light with deformable polymer layer in the second research, the results and discussion about these two projects will be explained in details with two sections.

3.1 The Movement of YAG:Ce on Melted Polymer

From the laser-based wetting angle measurement, the two kinds of melted polymer's wetting angle and the in-situ wetting angle measurement during the transportation process were obtained.

3.1.1 The Wetting Angle for Crystal Bond and Hot Melt Glue Stick

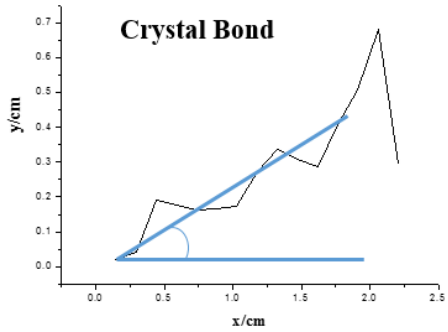

x: Position (cm)
y: $(x_{n+1}-x_n)\tan\alpha+y_n$

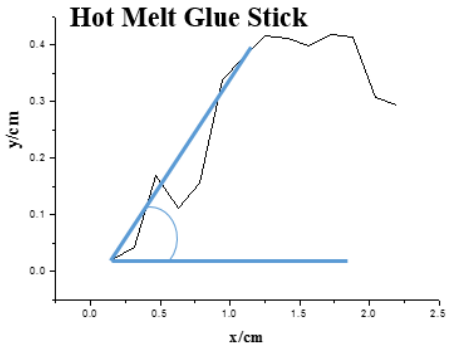

x: Position (cm)
y: $(x_{n+1}-x_n)\tan\alpha+y_n$

Figure 35: Wetting angle forming by two kinds of melted polymer.

The wetting angle of two kinds of polymers were measured with melt polymer heat-treated by the hot wire. In Figure 35 above, the polymer height y ($y_{n+1}=(x_{n+1}-x_n)\tan\alpha+y_n$) at each position (x/cm) was calculated with the angle α obtaining from the working principle shown in Figure 25, and all the heights at different position were gathered to obtain the surface profile and the wetting angle in a cross section view as well.

Clearly observed from the two wetting angles shown in Figure 35 above, the hot melt glue stick has a favourable wetting angle on the surface of applied glass substrate and therefore the ability to transport particles through the melt polymer upon heating can be ensured. Besides the wetting angle measurement, the transportation of YAG:Ce was only observed with hot melt glue stick instead of crystal bond.

3.1.2 The Transportation of YAG:Ce by Hot Melt Glue Stick

The ability to move particles was confirmed by wetting angle comparison between two kinds of polymers, and the image of the transportation process was also captured by a high resolution webcam.

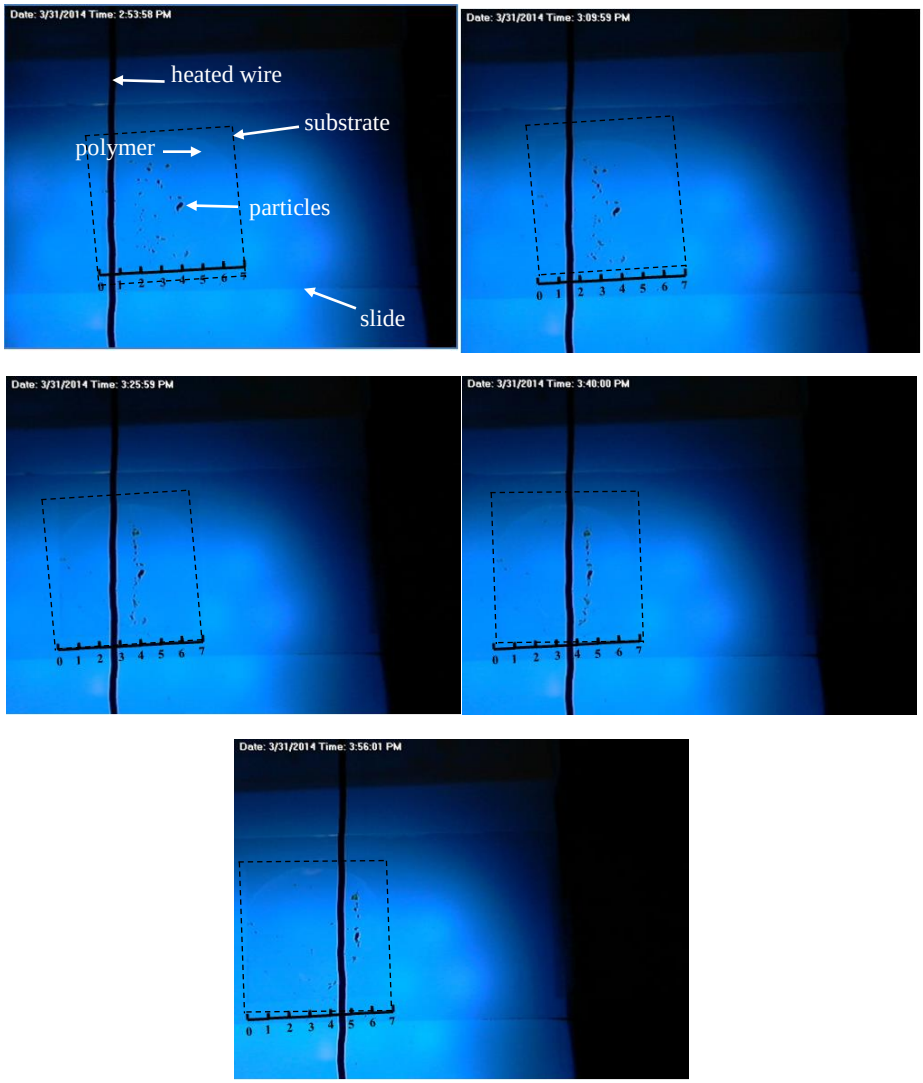

Figure 36: YAG:Ce particles moving (photos taken at 5 different times with time interval between photographs of 15 minutes, Scale shown is 3.1 mm per division).

A clear view of the transportation of YAG:Ce particles through melted hot melt glue stick was observed from the Figure 36 shown above. Through the wetting angle of melting polymer was measured at a given moment in time the hot wire was located on the top of approximately half of the melted polymer.

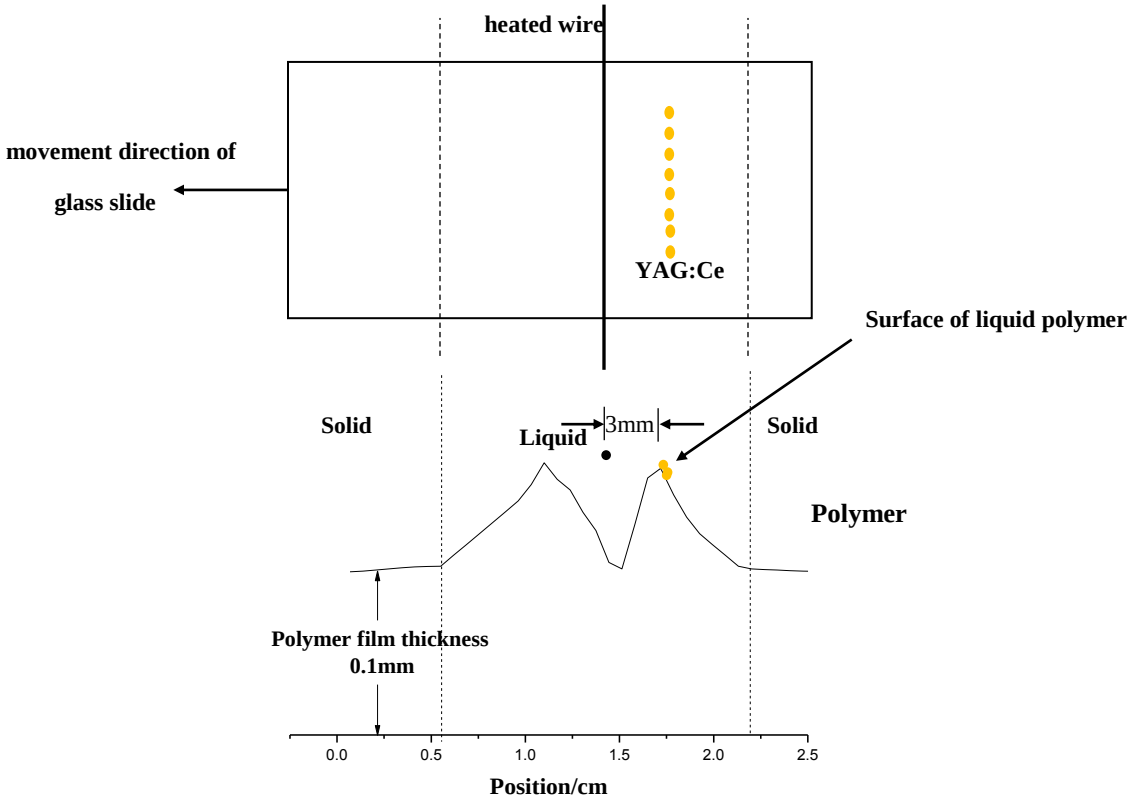

Figure 37: The melt and the solid polymer in a cross section view.

In the experiment, the melted glue stick polymer is observed to form a valley-like surface that is able to transport YAG:Ce powder particles much like a surfer is carried forward on a wave. As the heat source is moving across the polymer, each newly-heated region melts, while the previously-melted region begins to cool and solidify. The process occurs continuously so that the melt region travels the entire length of the polymer sample. At the surface of the liquid polymer, the floating YAG:Ce can be pushed forward by the advancing liquid front forming by the surface tension difference causing from the thermal gradient by the hot wire on the top.

3.1.3 In-Situ Wetting Angle during Transportation Process

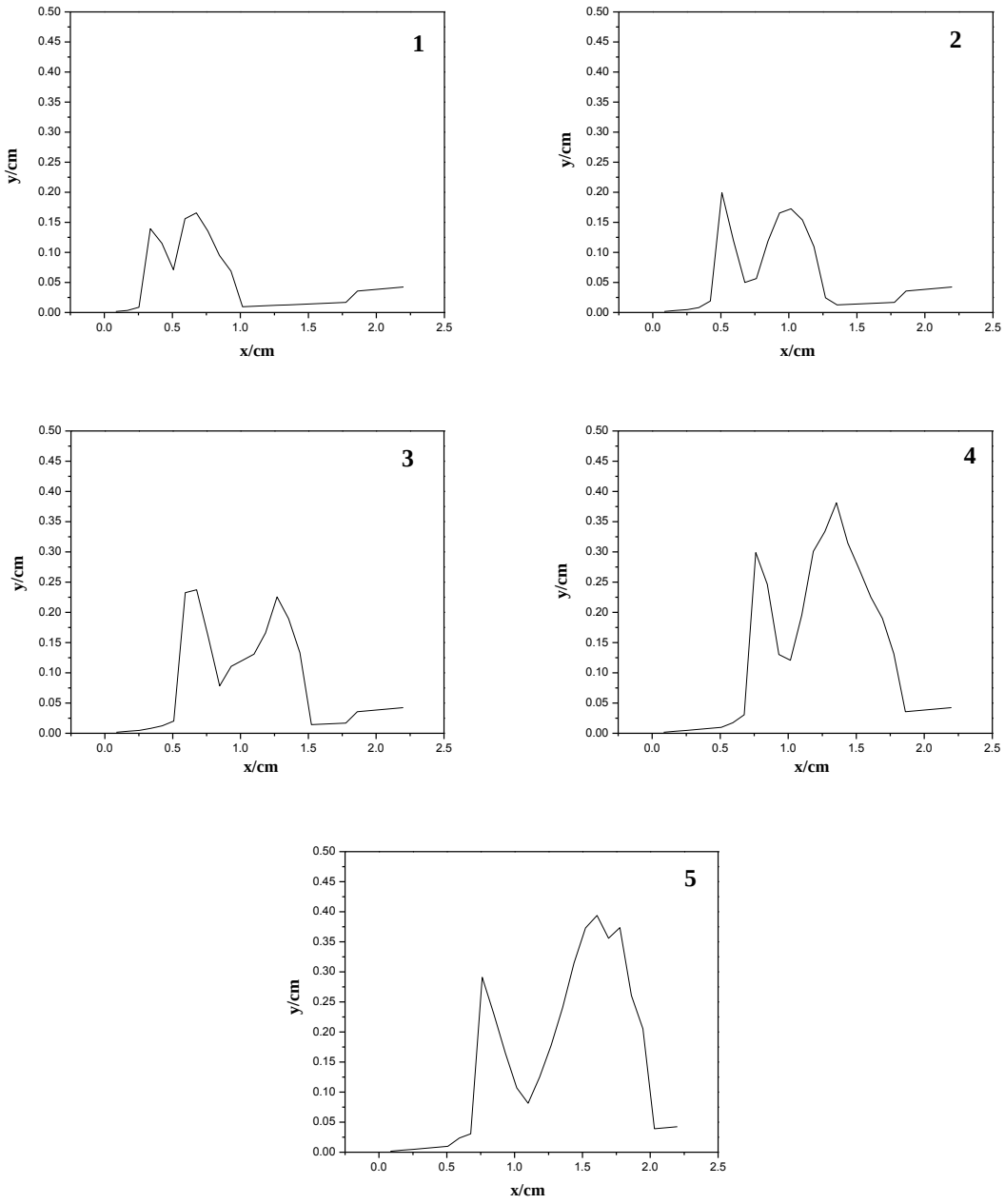

Figure 38: In-Situ wetting angle during the transportation process (from 1 to 5 by time order).

The same laser-based wetting angle measurement was applied during the YAG:Ce particles transportation process to observe the melted polymer functioning in a different view.

The two bumps shown in each surface profile is formed with the hot wire in the middle, not only the surface tension effect, of which the surface tension for molecules as a function of temperature in the center is lower than that on the sides, and the surface molecules with higher surface tension on the sides will pull the surface molecules in the center away from the central region, but the vaporization of polymer. Because the right bump was supporting the YAG:Ce particles in the experiment, the movement of the right bump from the 1st surface profile to the 5th surface profile can present the movement of the melted polymer, and the transportation of YAG:Ce particles as well.

Because of the inaccuracy existing in the wetting angle measurement, such as the reading of laser dot position by human errors, more precise method is required for obtaining the surface profile of the melted polymer in the future.

3.1.4 Various Polymer and Substrate Trials

Because of the high vaporization rate of the polymer when heated, another type of polymer material was chosen to replace the hot melt glue stick for tackling the high vaporization problem. PVB (Polyvinyl butyral) is a resin usually used for applications requiring optical clarity including laminated safety glass for automobile windshields [36]. When laminated under heat and pressure, the PVB interlayer becomes optically clear. In my experiment, one PVB layer from DuPont® was heat treated with a digital hot plate and the weight loss as the increasing temperature was also measured.

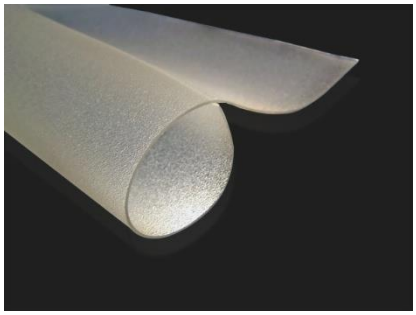

Figure 39: Opaque PVB film.

Starting with the weight of 0.203 g at room temperature, the opaque PVB film as shown above located on the same microscope cover glass on the top of the hot plate lost weight and became optically clear at around 70 ℃. When the temperature reached 120 ℃, the PVB film started to melt, followed by a colour change from clear to yellow and then burned at 150 ℃.

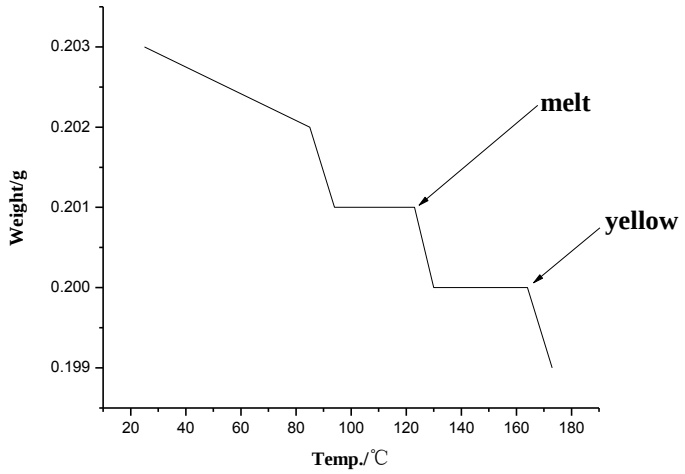

Figure 40: Weight loss of PVB film as the increasing temperature.

A microscope cover glass was applied for this experiment because of its ability to prevent excessive heat dissipation. However, the thermal conductivity of glass is 0.8 [37]

~ 1.05 [38] W m^{-1} K^{-1} at 293 K, which is high compared to the Polytetrafluoroethylene, Teflon (PTFE) of 0.25 [39] W m^{-1} K^{-1} at 293 K. In addition a glass cracking problem when the polymer layer on the top of the glass cools down was also observed during the experiment. Hence, one piece of Teflon sheet (thickness of 2 mm) as a substrate was used for the polymer heat-treated trial. The desired result was obtained without a substrate cracking problem and low excessive heat dissipation was ensured.

Therefore a desirable substrate yet to be identified and tested for this experiment has low thermal conductivity and high stress resistance, also with the optically clear property, which is required in the future work.

3.2 The Polymer-Based Deformable Lens for Solar Tracking

The focal property of the polymer-based deformable lens is highly dependent on the surface tension difference caused from the thermal gradient from the center to the side where the ITO glass heating source was located. The surface temperature profile of the ITO heating source was measured at the beginning.

3.2.1 The Surface Temperature Profile of ITO Heating Source

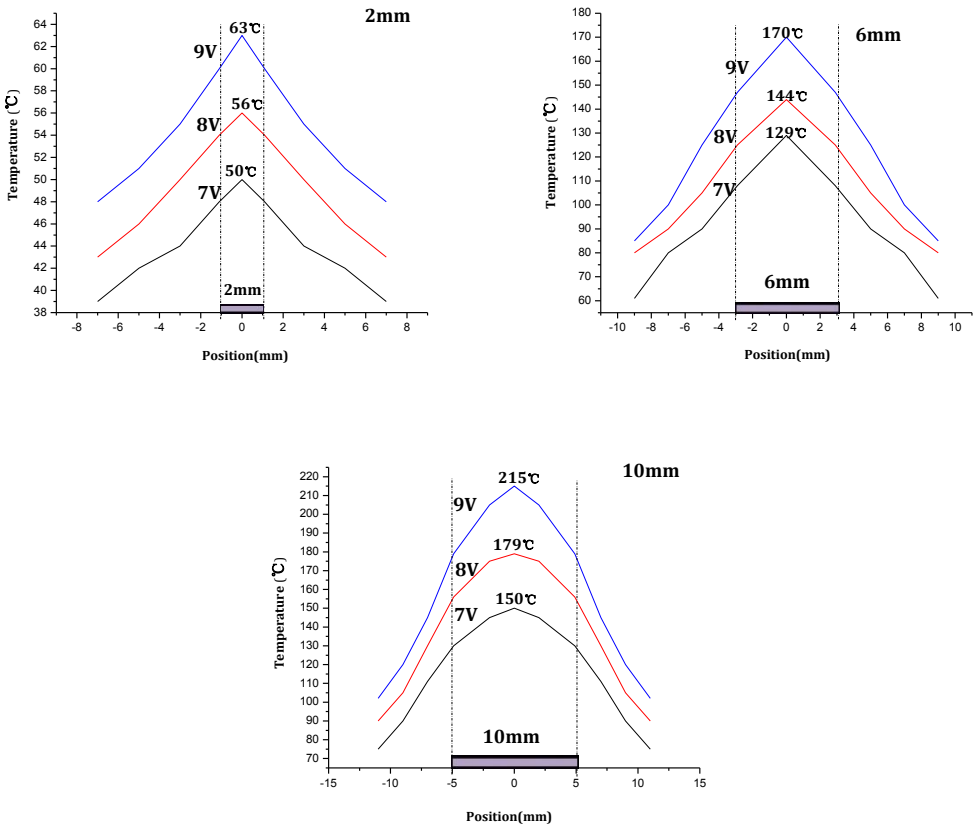

Figure 41: The surface temperature of ITO heating source (2 mm, 6 mm and 10 mm width ITO stripe) at 7 V, 8 V and 9 V.

With the assistance of J-type thermocouple with a diameter of 76.2 μm, the temperature in one specific point could be read precisely. In the temperature profile, the

highest temperature was shown on each peak and the ITO stripes with different width were also adding to indicate the center and side position. According to the plot, the temperature increased with the increasing ITO stripe width and heating power, and decreased from the center to the side, which forming a thermal gradient, resulting in a surface tension gradient.

3.2.2 COMSOL Multiphysics Modelling for Surface Temperature Profile

Using the COMSOL Multiphysics modelling software, a heating source (modelled as a heat flux) with a width of 2 mm, 6 mm and 10 mm and a height of 1 mm at different heating powers located in the middle and with another two rectangles on the side was modelling in 2D view. The chosen material is Corning® 1737 glass as the same as the material of ITO coated glass substrate. The whole width is 1.5" (0.0381 m), which is surrounding with air. The heat transfer coefficient of the top surface excluding the heating source area is 10 W/(m^2·K) and 6 W/(m^2·K) for the bottom surface. The surface temperature profile through this modelling can be shown in both 2D and 1D plot.

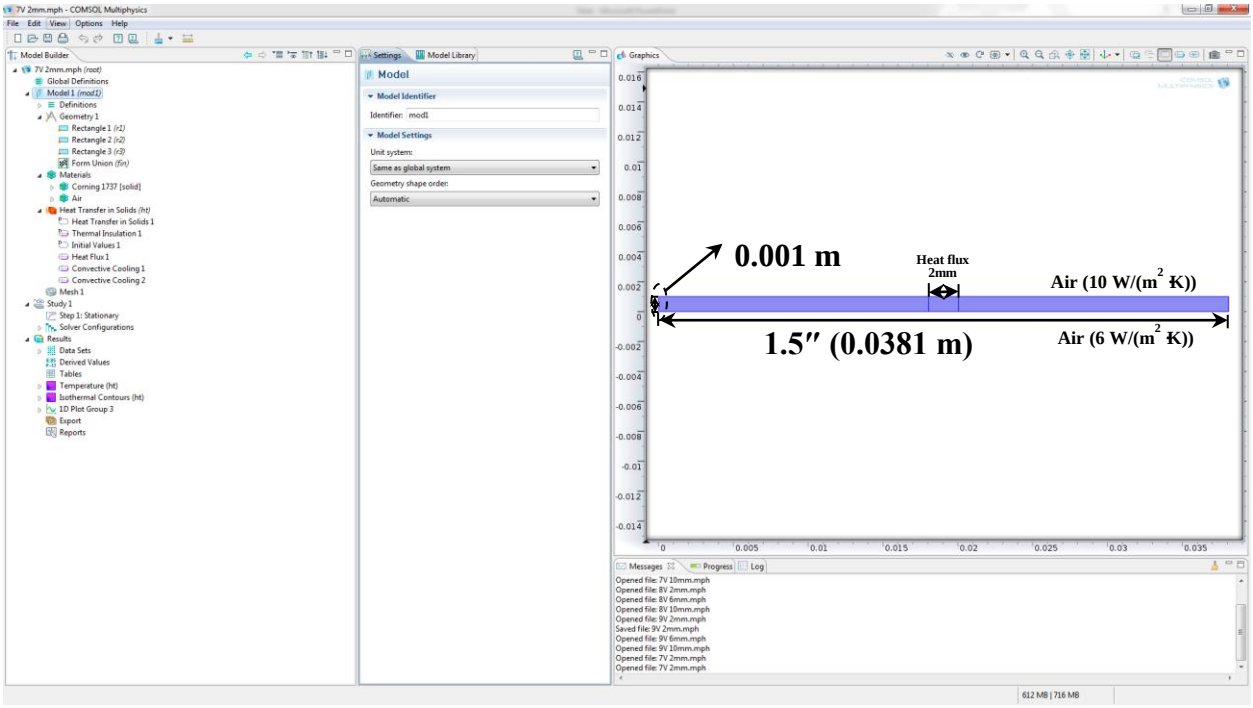
0.001 m
Heat flux
2mm
Air (10 W/(m^2 K))
1.5″ (0.0381 m)
Air (6 W/(m^2 K))

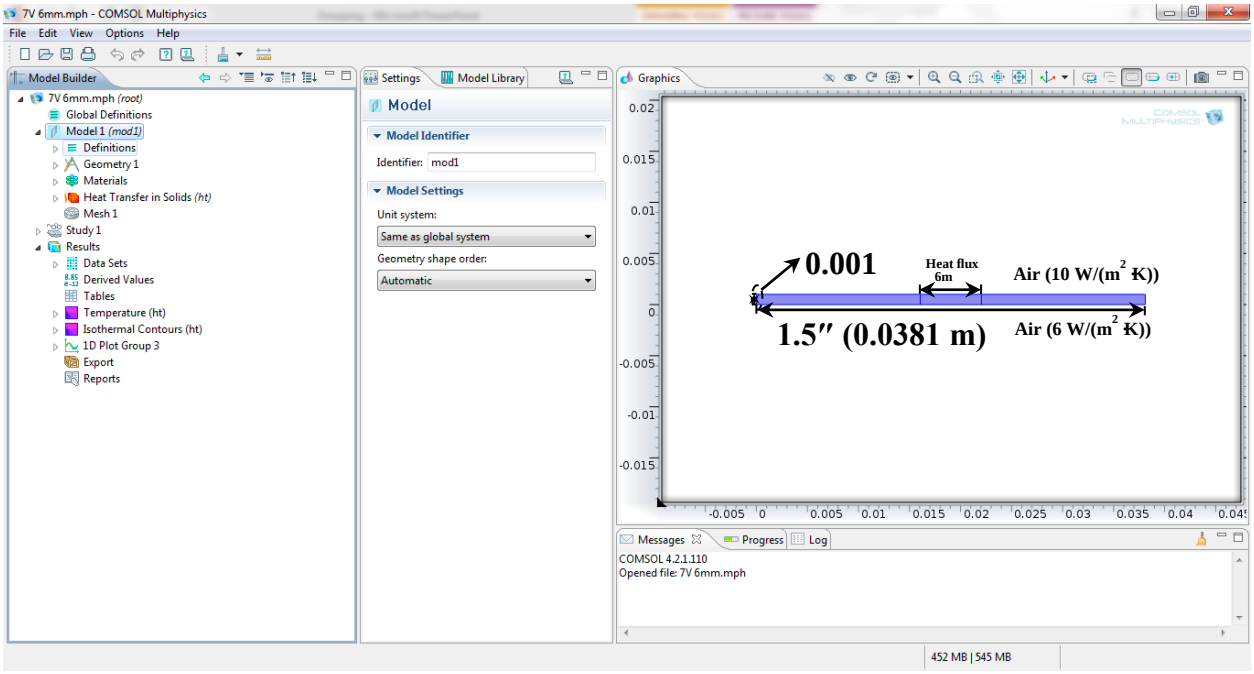
7V 6mm.mph - COMSOL Multiphysics
File Edit View Options Help
Model Builder
Settings
Model Library
Graphics
Model
Model Identifier
Identifier: mod1
Model Settings
Unit system:
Same as global system
Geometry shape order:
Automatic
0.001
Heat flux
6m
Air (10 W/(m^2 K))
1.5″ (0.0381 m)
Air (6 W/(m^2 K))
Messages
Progress
Log
COMSOL 4.2.1.110
Opened file: 7V 6mm.mph
452 MB | 545 MB

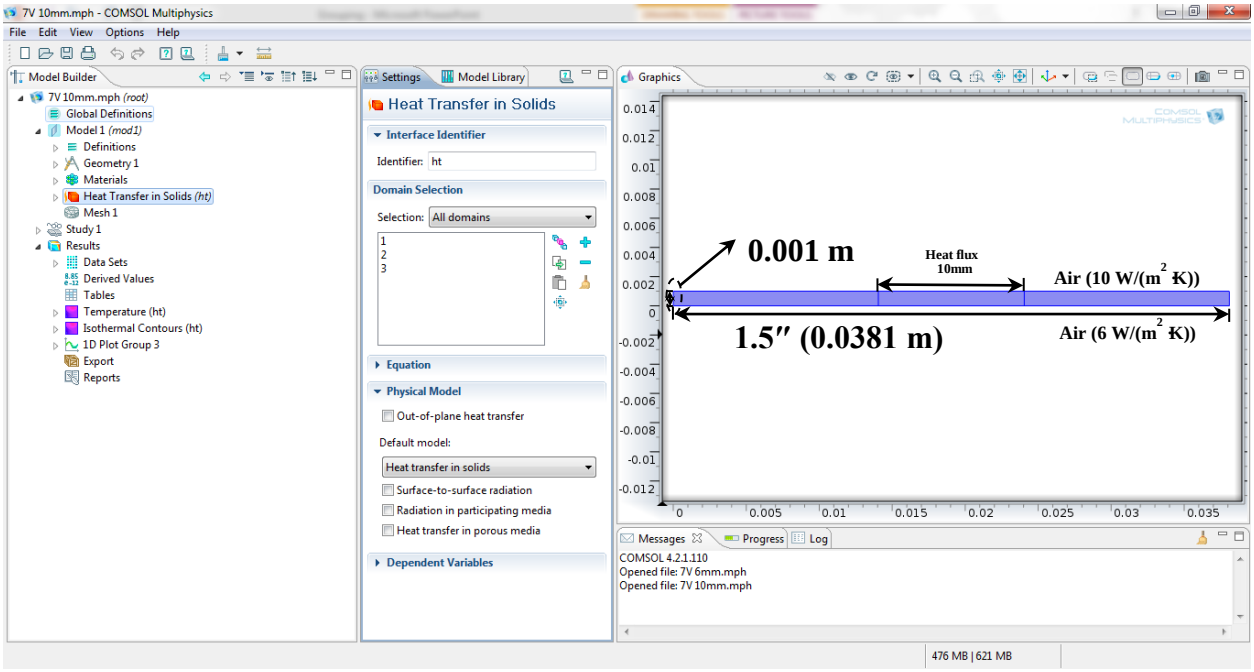

Figure 42: Snapshot of COMSOL Multiphysics modelling (the dimensions of the heating source as shown).

The heating flux for each size ITO heating source at different heating power was also shown in the Table 3 below, representing heat supplied in the center position with the equation of total heating flux q_{tot}, ($q_{tot} = \frac{V(Voltage) \times I(Current)}{0.0381m(length)}$).

Table 3: Total heat flux for different width ITO stripe at various heating power (voltage times current).

Width/heating voltage	7 V	8 V	9 V
2 mm	11.02 W	12.60 W	14.17 W
6 mm	33.07 W	37.80 W	42.52 W
10 mm	55.12 W	62.99 W	70.87 W

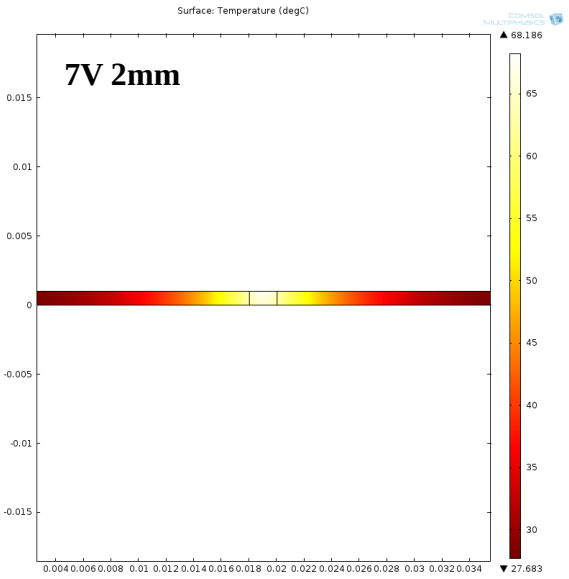
Surface: Temperature (degC)
7V 2mm
▲ 68.186
▼ 27.683

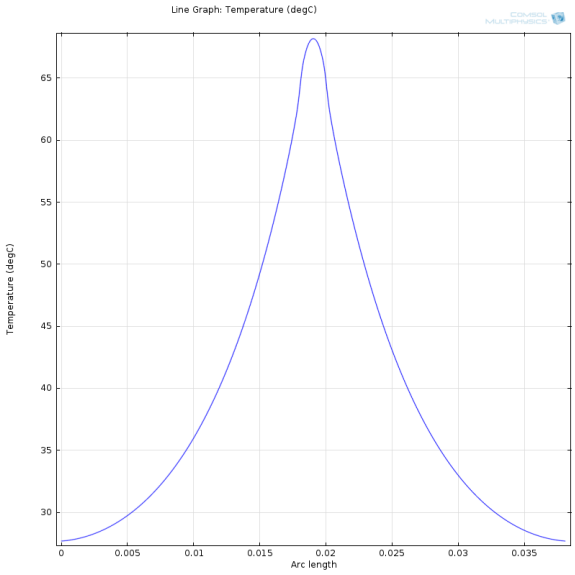
Line Graph: Temperature (degC)
Temperature (degC)
Arc length

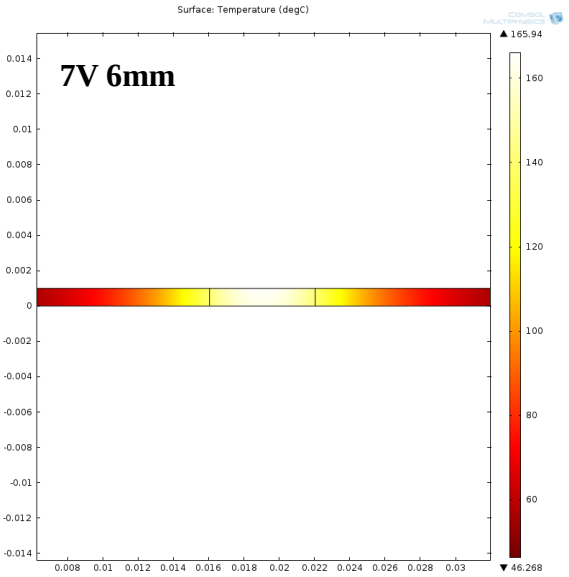
Surface: Temperature (degC)
7V 6mm
▲ 165.94
▼ 46.268

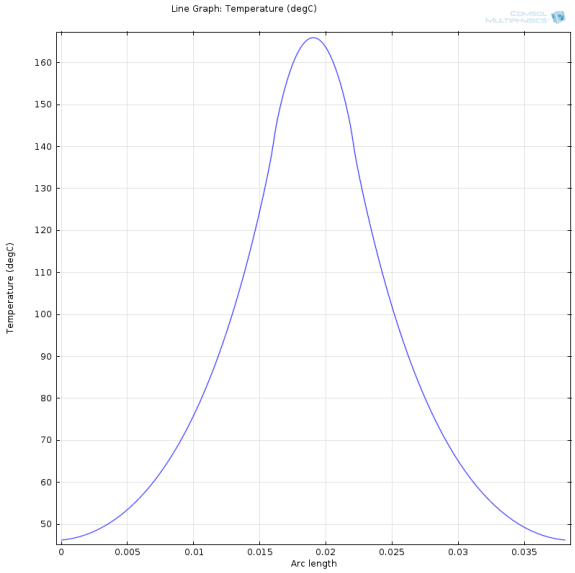
Line Graph: Temperature (degC)
Temperature (degC)
Arc length

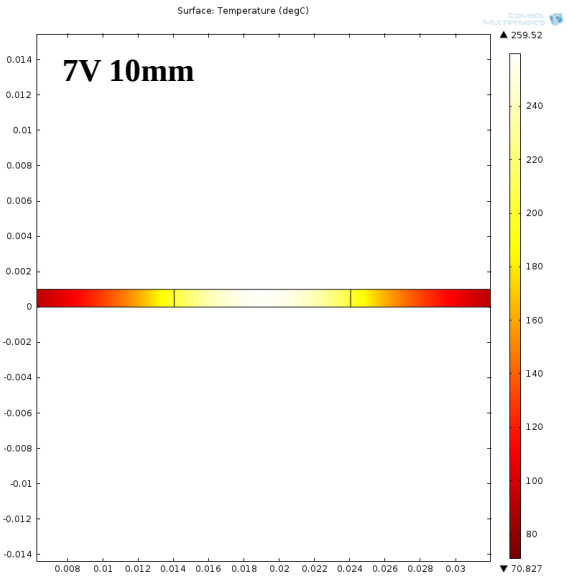
Surface: Temperature (degC)
7V 10mm
▲ 259.52
▼ 70.827

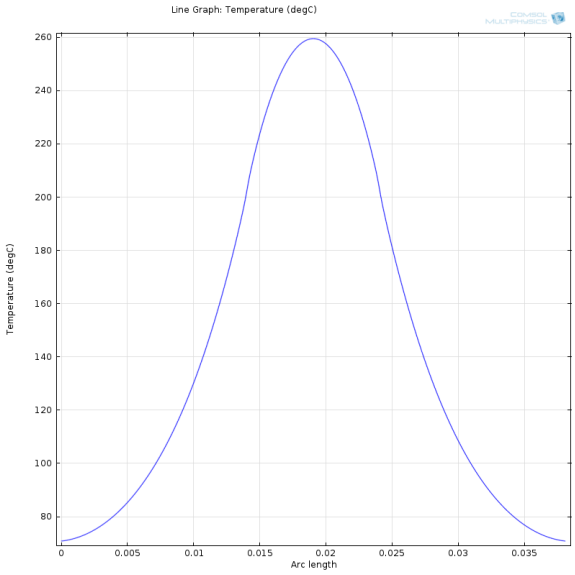
Line Graph: Temperature (degC)
Temperature (degC)
Arc length

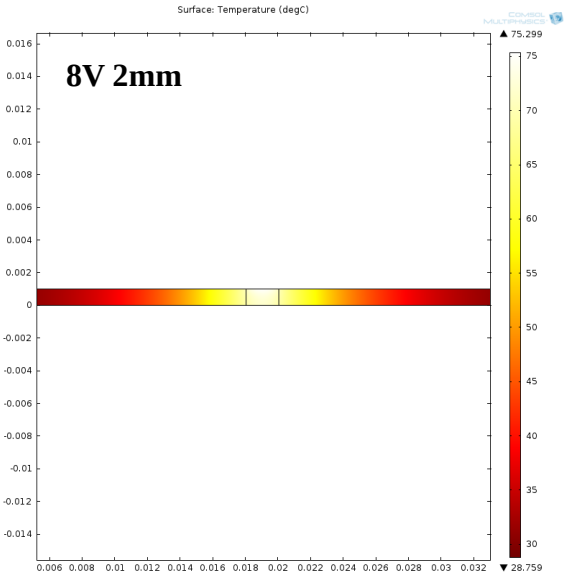
Surface: Temperature (degC)
8V 2mm
▲ 75.299
▼ 28.759

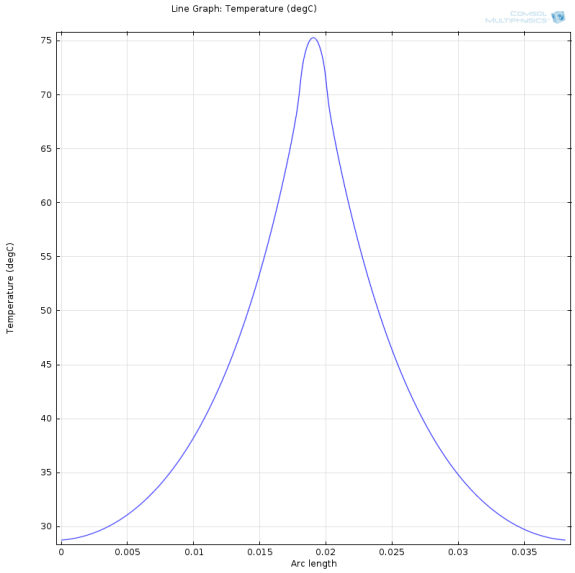
Line Graph: Temperature (degC)
Temperature (degC)
Arc length

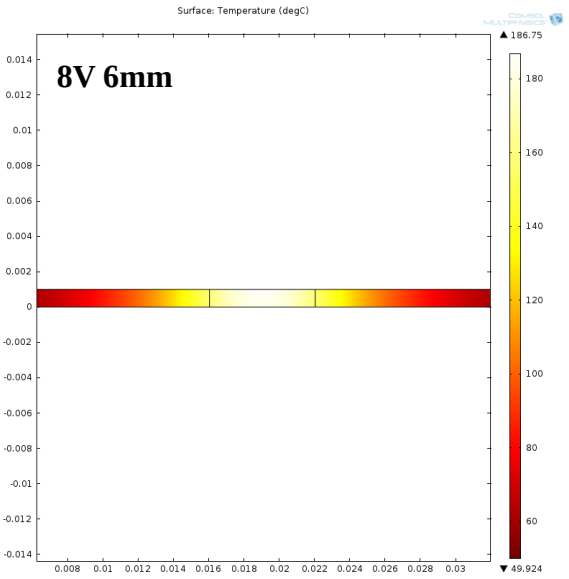
Surface: Temperature (degC)
8V 6mm
▲ 186.75
▼ 49.924

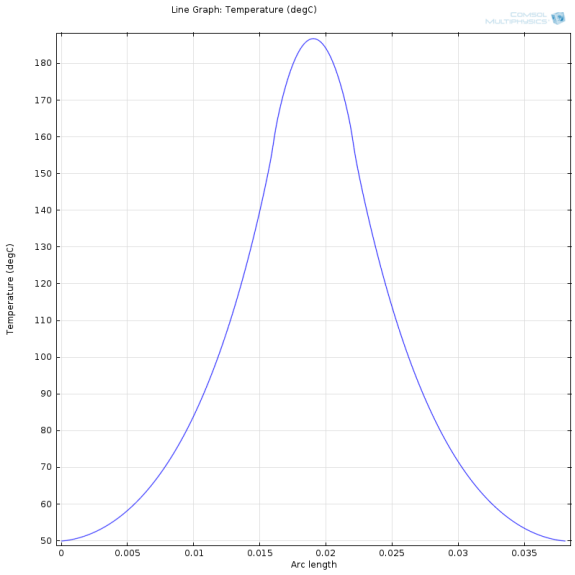
Line Graph: Temperature (degC)
Temperature (degC)
Arc length

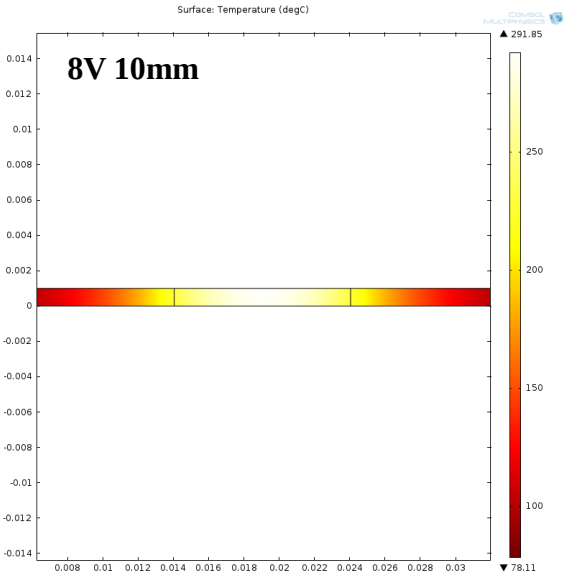
Surface: Temperature (degC)
8V 10mm
▲ 291.85
▼ 78.11

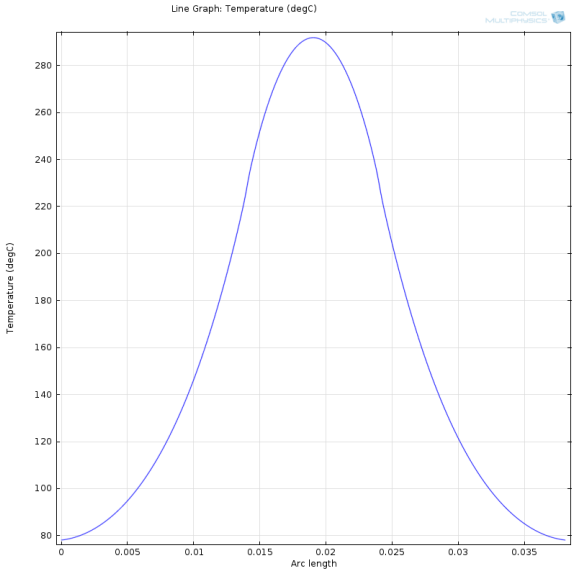
Line Graph: Temperature (degC)
Temperature (degC)
Arc length

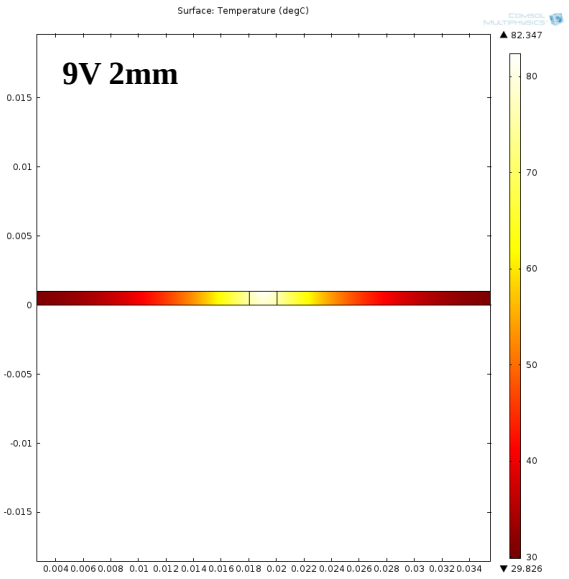
Surface: Temperature (degC)
9V 2mm
▲ 82.347
▼ 29.826

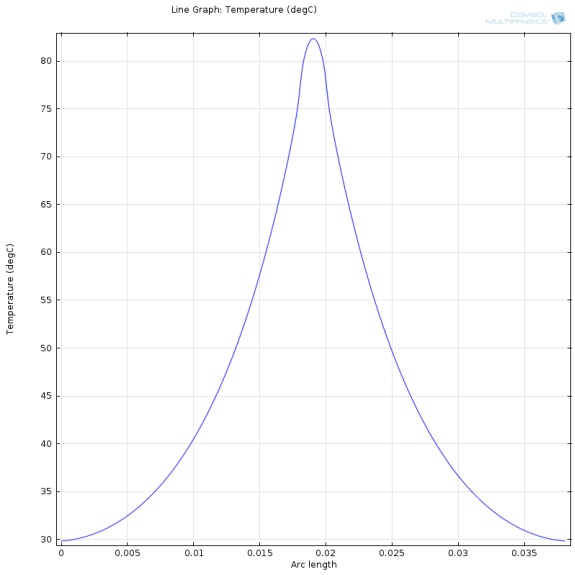
Line Graph: Temperature (degC)
Temperature (degC)
Arc length

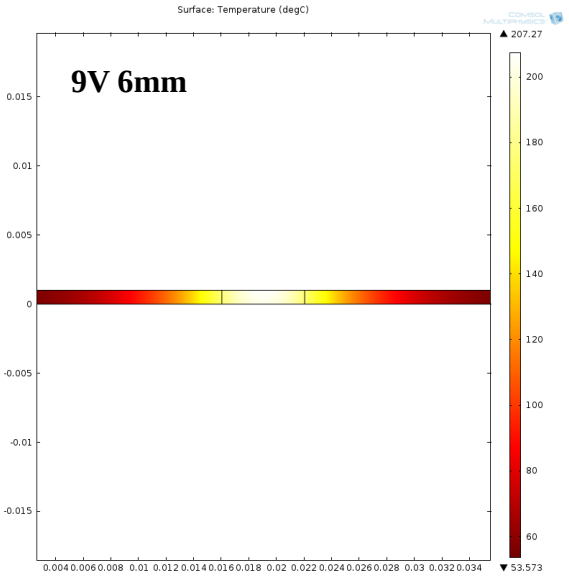
Surface: Temperature (degC)
9V 6mm
▲ 207.27
▼ 53.573

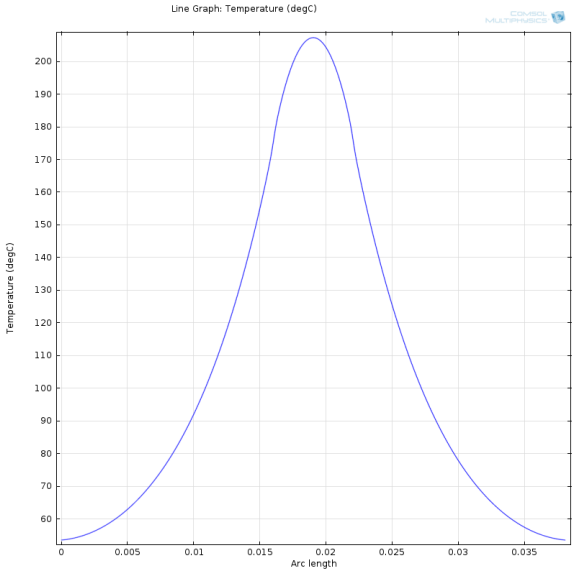
Line Graph: Temperature (degC)
Temperature (degC)
Arc length

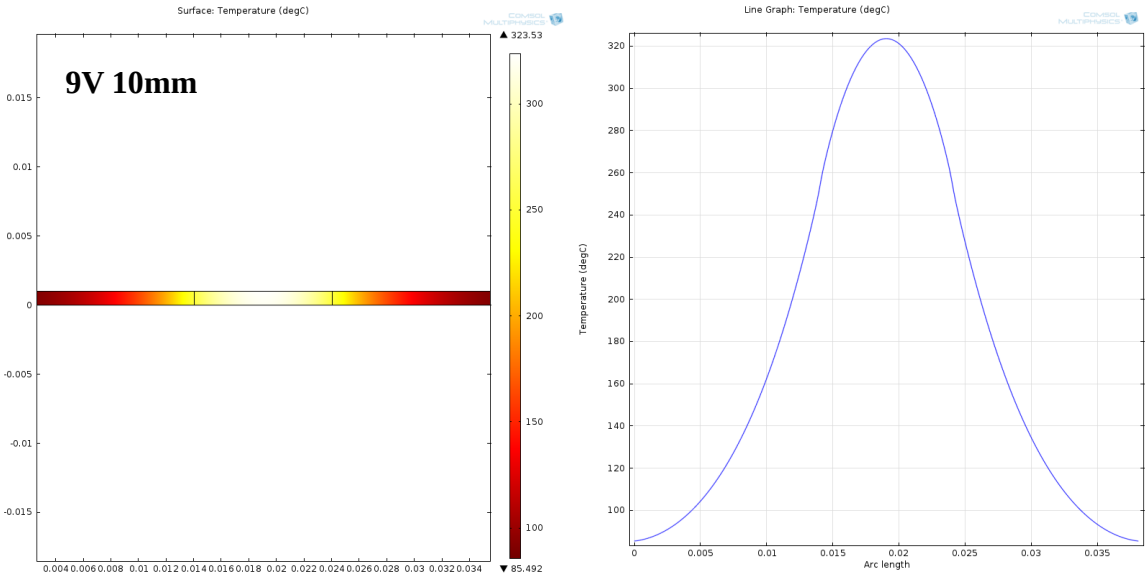

Figure 43: 2D and 1D plot of surface temperature profile according to the position from the center to the side for 2 mm, 6 mm and 10 mm stripe width ITO heating source at the heating power of 7 V, 8 V and 9 V.

From the modelling plot above, the thermal gradient that temperature decreased from the center to the side is compared favourably to what was measured by the thermocouple. With wider ITO stripes at higher heating power, the temperature was also higher as shown. However, the modelling temperature was higher than the experimental measurement, such as 18 ℃ higher for the 2 mm ITO stripe at 7 V and 108 ℃ higher for the 10 mm ITO stripe at 9 V. The temperature difference between the modelling reading and experimental measurement was also increasing with the increasing heating power and ITO stripe width. There are several reasons for the difference: for the modelling reading, the heating source model was applied by the way of heat flux instead of heat generation directly from the ITO stripe as in reality because of the difficulty to realize the micron scale of ITO film in the modelling software, and the chosen heat transfer coefficient for the top surface and the bottom surface are not precise. For the experimental measurement,

there should be heat dissipation between the thermocouple and the surface of ITO stripe even though the silicone paste was applied, which also led to the difference from the actual temperature.

3.2.3 Light Concentrating Results

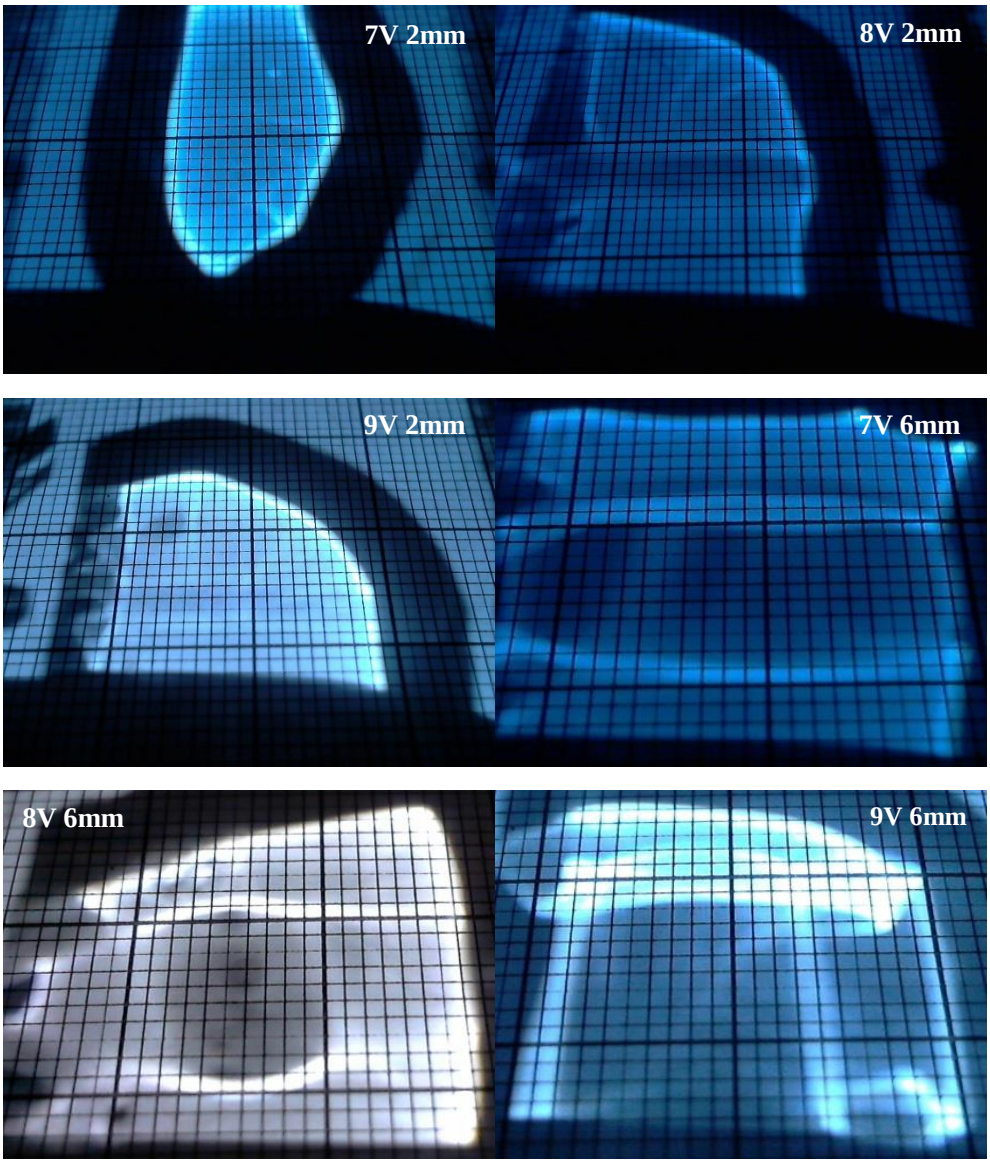

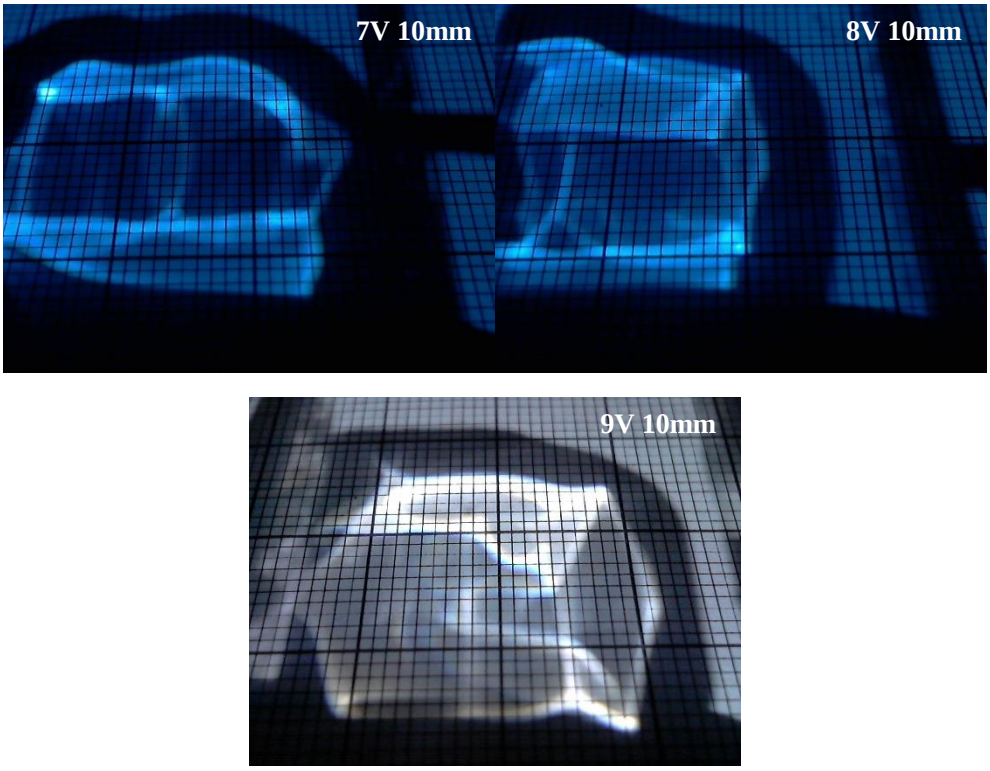

Figure 44: Light focusing image of Polystyrene with Toluene generating lens on the 2 mm, 6 mm and 10 mm stripe width ITO heating source at different voltage.

Light focusing images of Polystyrene with toluene solvent are shown above. With higher voltage, the focusing line becomes sharp and brighter. Because more heat is supplied with 9 V across the ITO stripe, the heating polymer has flowed further than it did at lower voltage, and polymer spread in a disorderly manner with unexpected light focusing regions.

For the 2 mm ITO stripe at all voltages, no obvious light focusing results initiated. From the Table 2 with the heating power applied at 7 V, the heat generating from the 2 mm ITO stripe is not sufficient to deform the polymer.

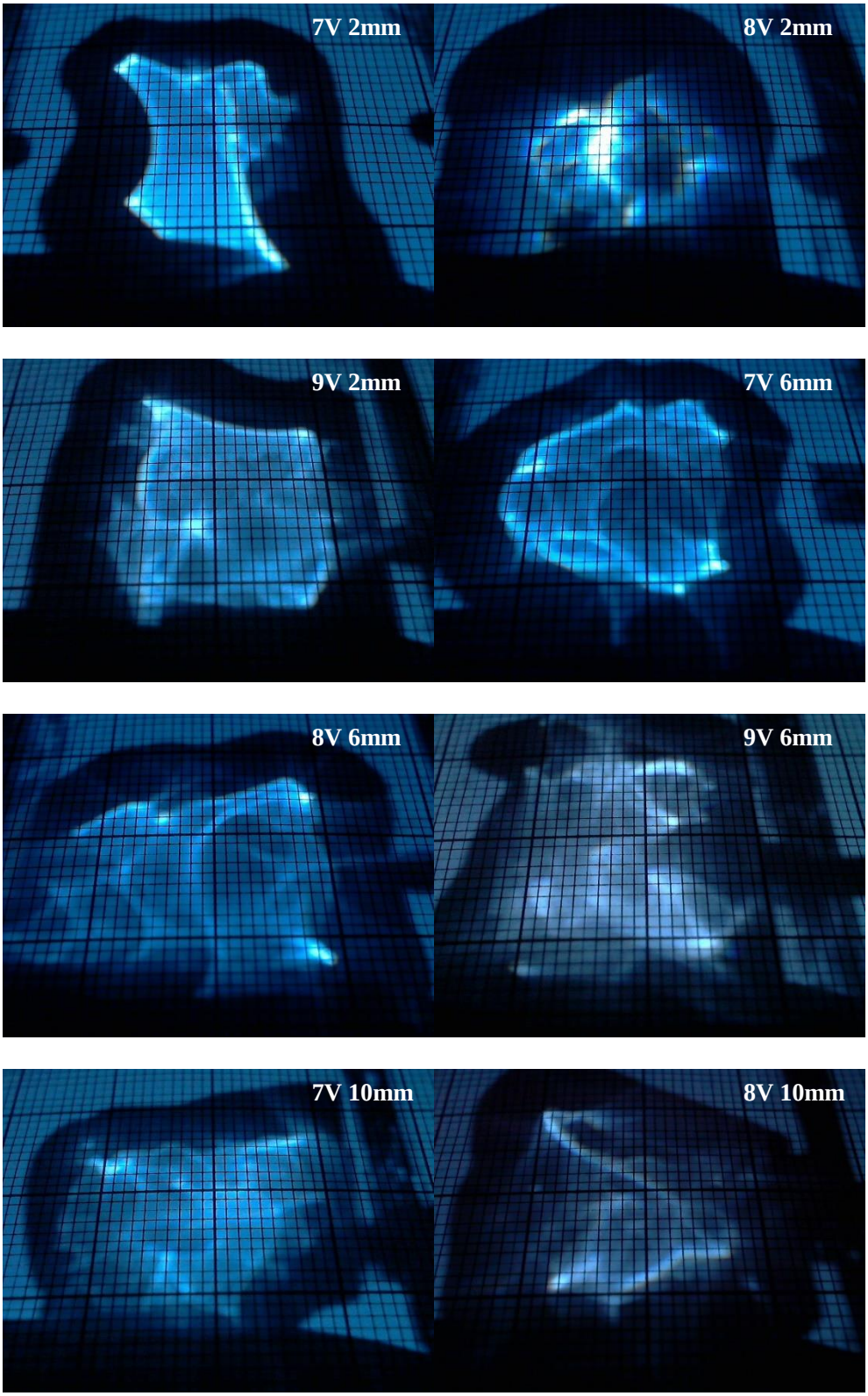
7V 2mm
8V 2mm
9V 2mm
7V 6mm
8V 6mm
9V 6mm
7V 10mm
8V 10mm

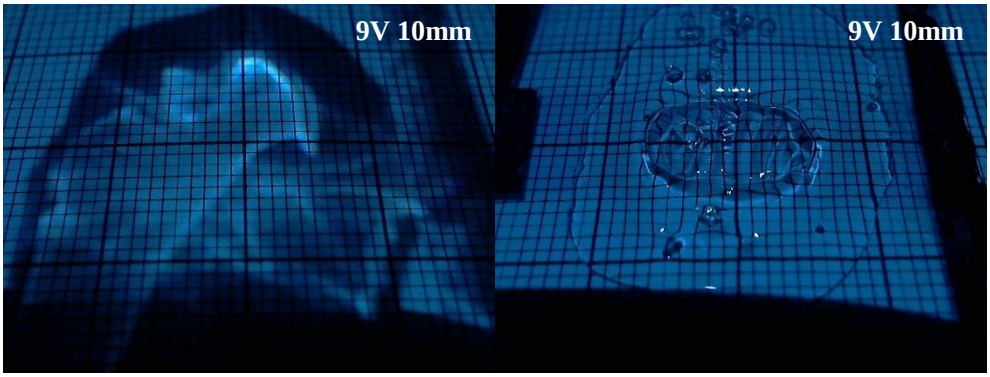

Figure 45: Light focusing image of Polystyrene with Tetrahydrofuran generating lens on the 2 mm, 6 mm and 10 mm stripe width ITO heating source at various voltages and the top view of polymer on the 10 mm stripe width ITO heating source at 9 V after heat treat experiment.

We observed the same trend with the polystyrene with toluene solvent. The polymer sample consisting of polystyrene and tetrahydrofuran also show non-light focusing on the 2 mm stripe width ITO heating source and disordered focusing results at the 9 V. However, the vapor pressure of tetrahydrofuran (132 mmHg at 20 ℃) is much higher than that (21 mmHg) of toluene, causing different diameters of bubbles occurring during the heating process, scattering severely light transmission. The bubbles could be observed from the last picture of the top view of the polymer sample above. The same problem was also bothering the polymer sample consisting of the polystyrene and chloroform as shown in figures below. Because of unstable power of LED light source positioning on the top and the webcam facing the axis paper for recording the focal results, the shown image background is not uniform, changing between bright blue and dark gray.

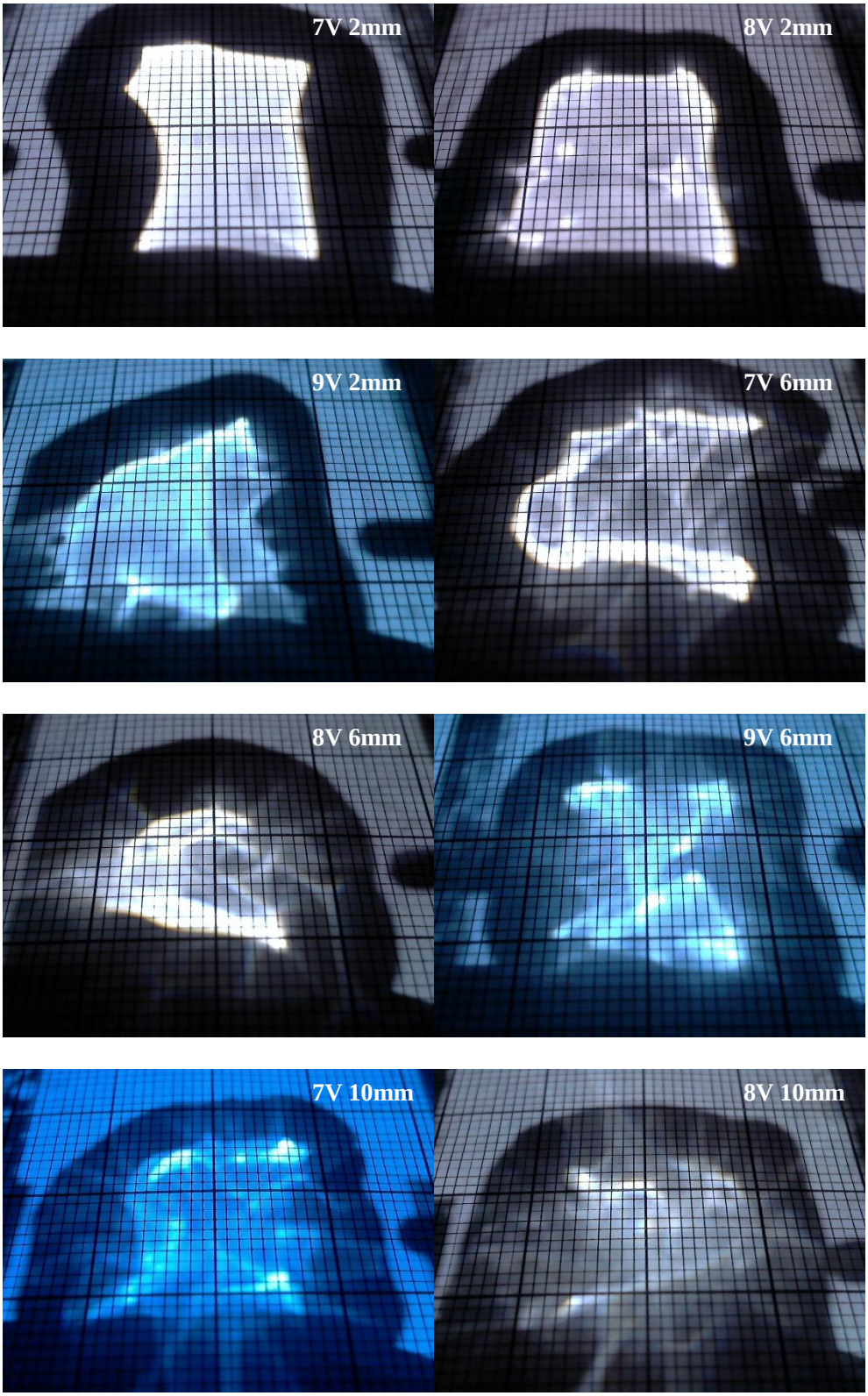
7V 2mm
8V 2mm
9V 2mm
7V 6mm
8V 6mm
9V 6mm
7V 10mm
8V 10mm

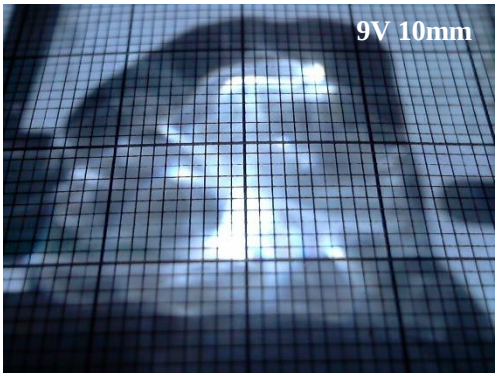

Figure 46: Light focusing image of Polystyrene with Chloroform generating lens on the 2 mm, 6 mm and 10 mm stripe width ITO heating source at different voltage.

3.2.4 Polymer Surface Profile

The polymer flow relies on the dilution effect of the solvent in the polymer during heating. Starting from a smooth cast polymer of uniform thickness, the polymer-based lens containing of two bumps is generated by the combination of Rayleigh-Bénard convection and Bénard-Marangoni flow effect.

When heat was provided from the bottom of the polymer layer in the center, high temperature polymer was expanded with lower density, ascending to the top because of buoyancy. And polymer on the top surface with higher density descended to the bottom because of gravity, heat will transfer through the mass flow convection between the top surface and bottom, and the surface tension for molecules as a function of temperature in the center is lower than that on the sides. With higher surface tension, the surface molecules on the sides will pull the surface molecules in the center away from the central region, causing the formation of two bumps.

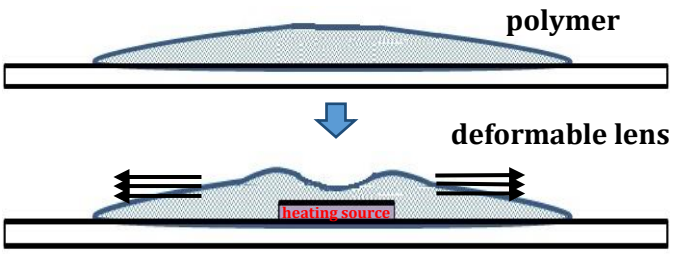

Figure 47: Schematic of formation of polymer-based lens.

In Figure 48 below shows the resulting polymer profile after a heating cycle for Polystyrene with toluene solvent on the 2 mm, 6 mm and 10 mm stripe width ITO heating source at different voltage. Combing with the light focusing image shown above, the sharp and brighter line was observed from the polymer-based lens sample on the wider ITO stripe at higher voltage. No obvious lens occurs for the polymer on the 2 mm wide ITO stripe.

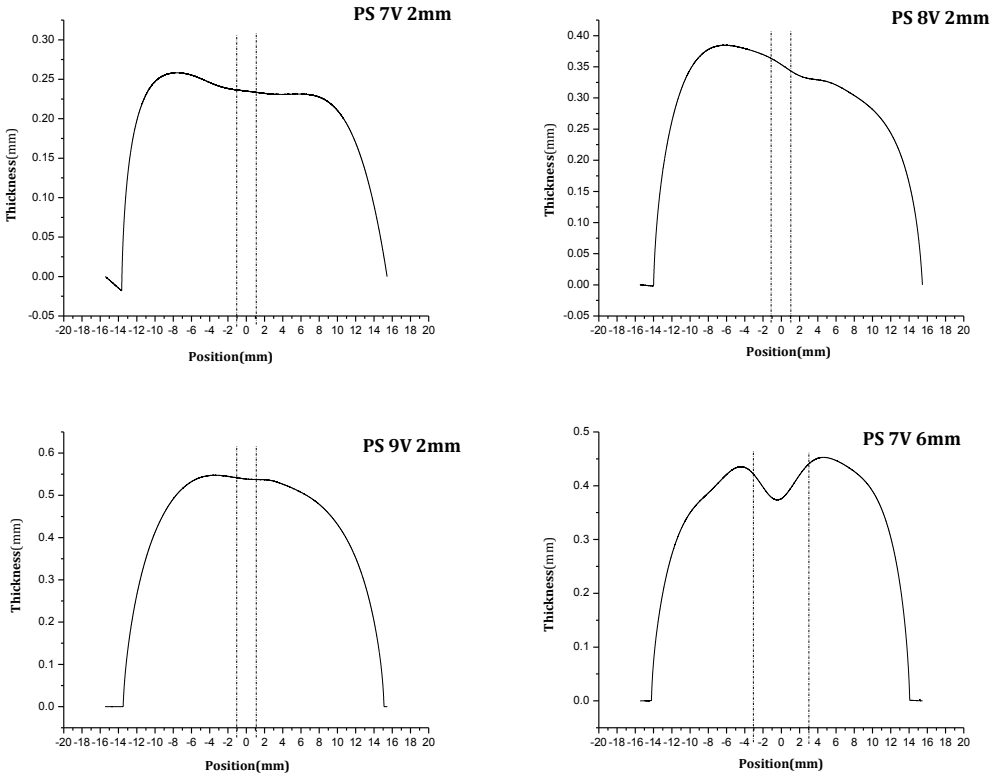

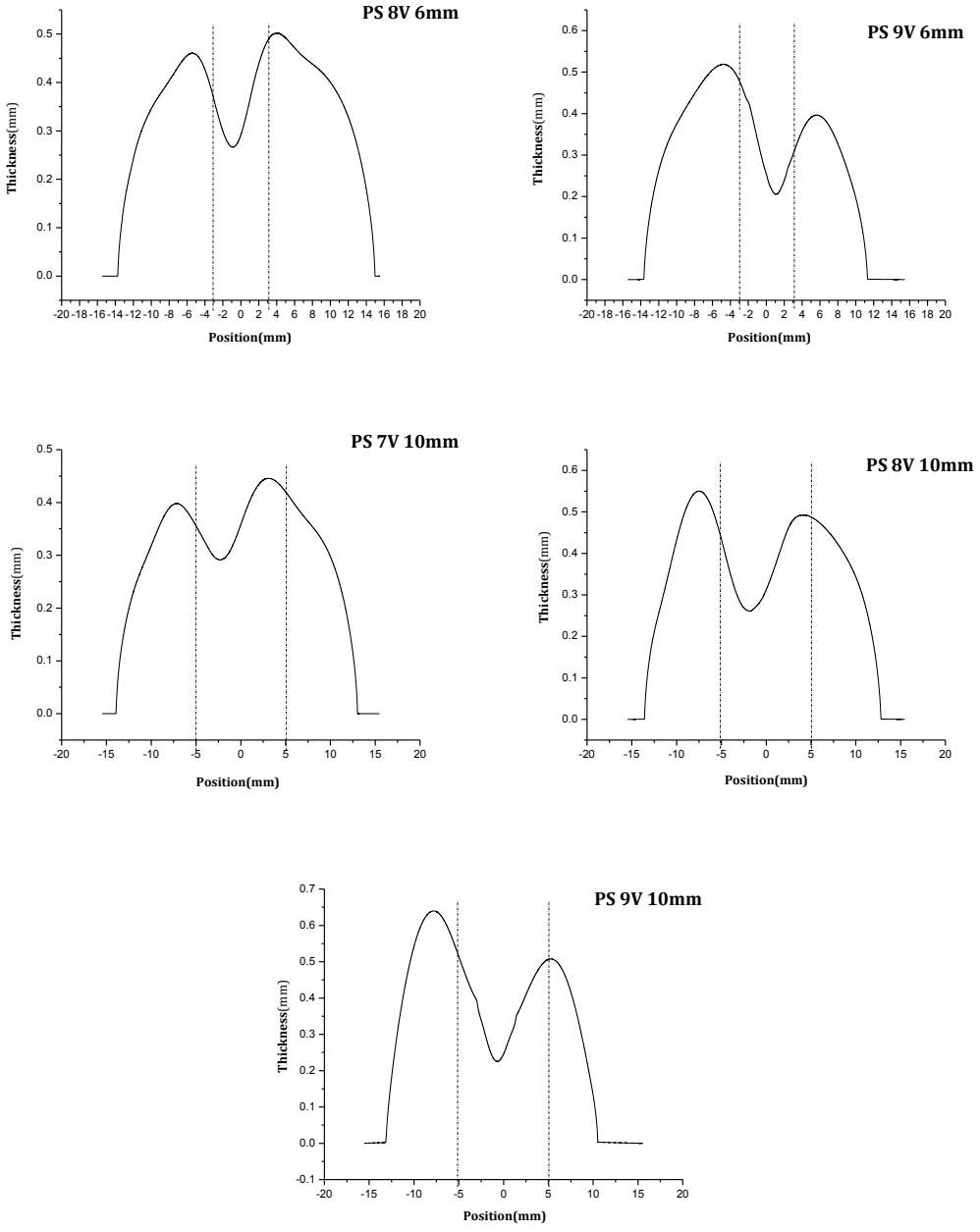

Figure 48: The surface profile of polymer-based lens (toluene as solvent).

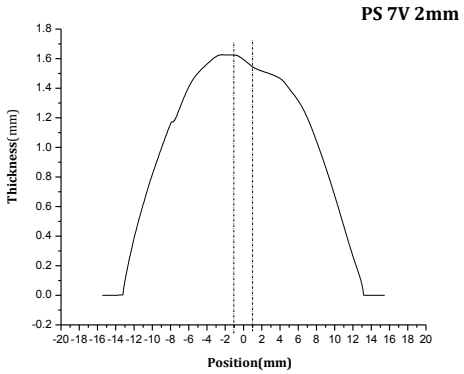
PS 7V 2mm
Thickness(mm)
Position(mm)

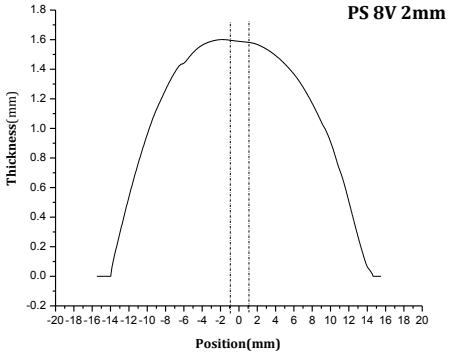
PS 8V 2mm
Thickness(mm)
Position(mm)

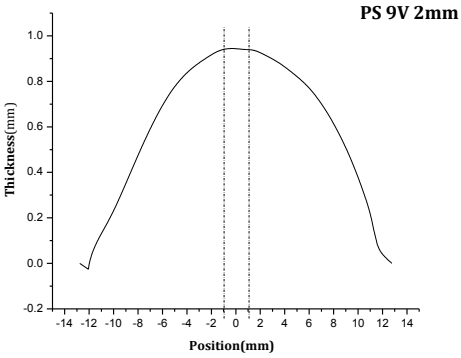
PS 9V 2mm
Thickness(mm)
Position(mm)

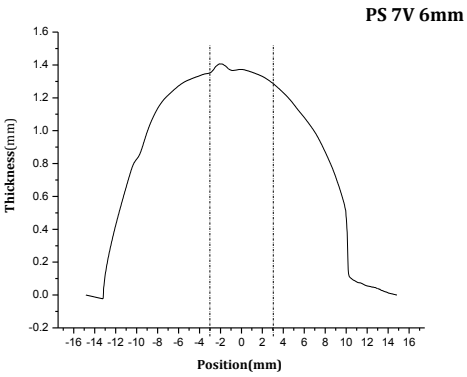
PS 7V 6mm
Thickness(mm)
Position(mm)

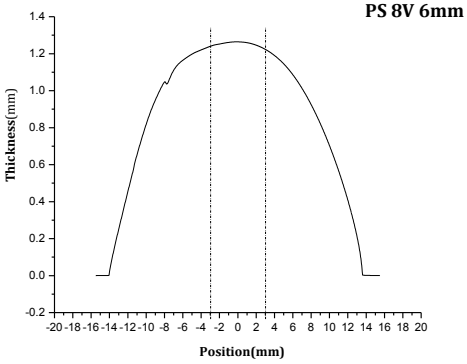
PS 8V 6mm
Thickness(mm)
Position(mm)

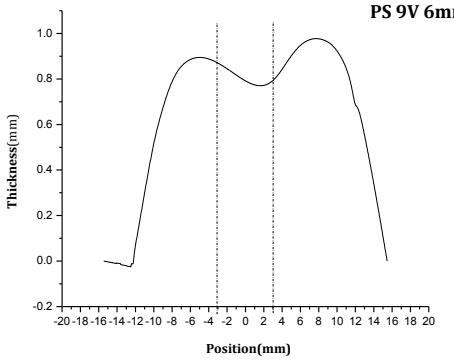
PS 9V 6mm
Thickness(mm)
Position(mm)

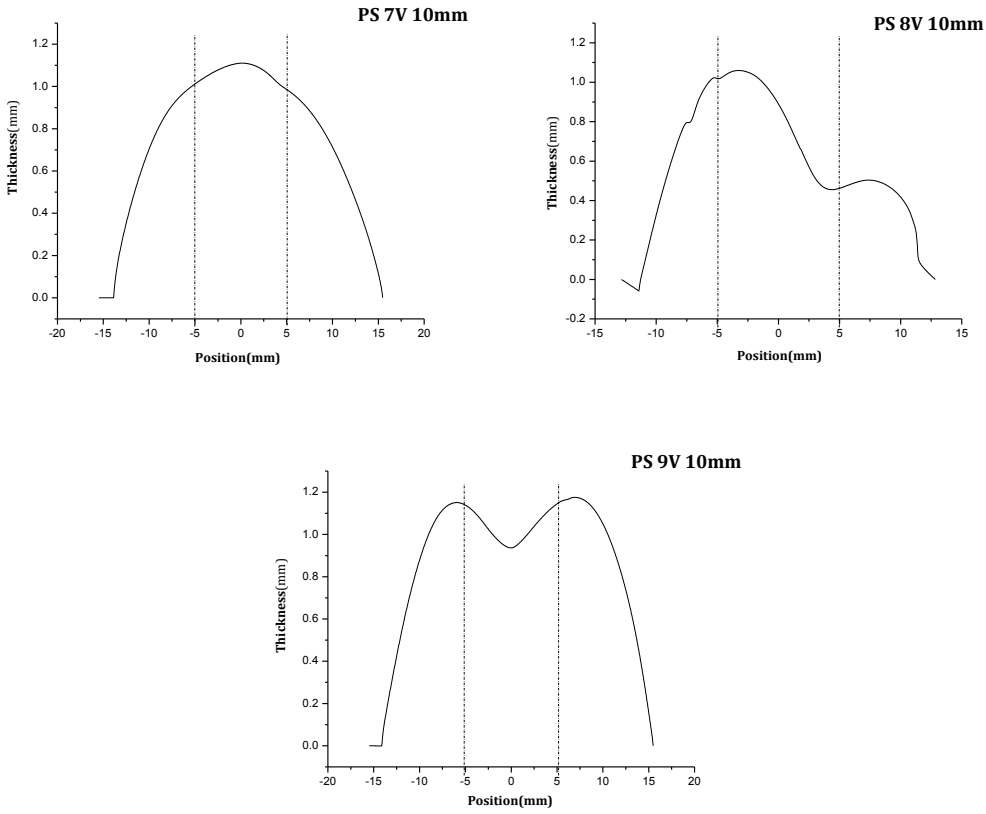

Figure 49: The surface profile of polymer-based lens (tetrahydrofuran as solvent).

From the focusing image shown in Figure 45 for the polymer sample with tetrahydrofuran as solvent, bubbles scattered the light so severely that few good enough light focusing results were obtained. Also, surface profiles for those polymer samples are formed more deeply. Bumps were only observed with the voltage of 8 V on the 10 mm ITO stripe and of 9 V on the 6 mm and 10 mm ITO stripes. The high vapor pressure leaves little amount of solvent in the polymer sample, which raises the viscosity of the melted polymer and made the polymer flowing more difficult.

3.2.5 Focal Length of Polymer Lens and Image Distance (i) Determination

As one of the most important properties of the lens, the focal length is determined using the surface profile shown above.

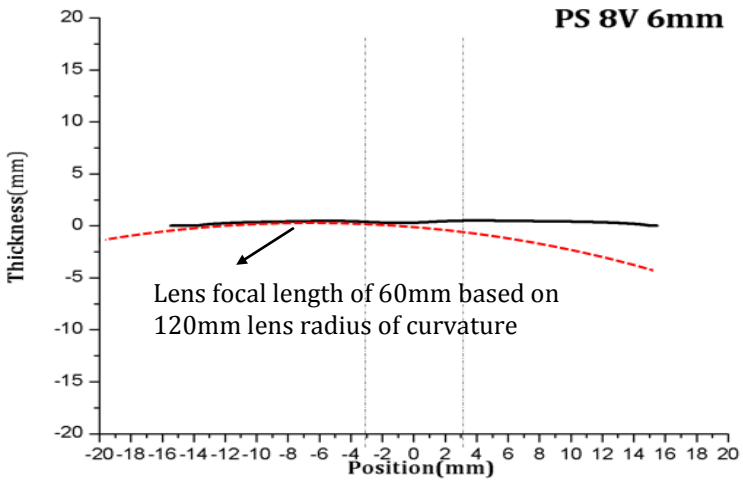

Figure 50: The focal length of Polystyrene generating lens with toluene as solvent on the 6mm ITO stripe at 8 V.

Based on the original surface profile of the polystyrene-toluene polymer sample, the focal length is 60 mm, half of the lens radius of curvature of 120 mm.

Also with the same polymer sample and by adjusting the position of axis paper, the focussed image distance (i: the distance between the lens and the screen) can be determined when the peak luminance indicating focusing of the sharp line is the highest reading from the photometer.

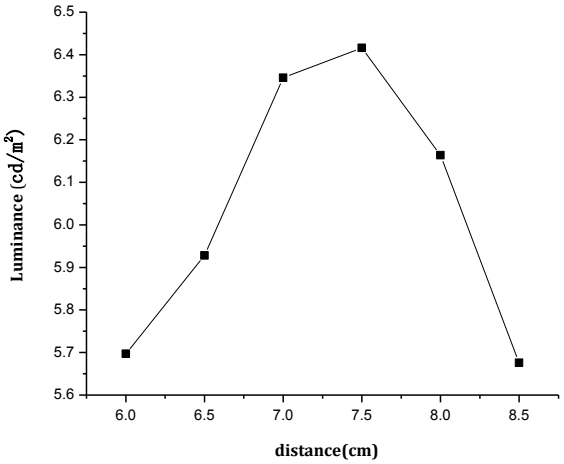

Figure 51: The luminance of Polystyrene generating lens with toluene as solvent on the 6mm ITO stripe at 8 V at different distance from the axis paper.

From Figure 51, the luminance is highest when the distance between the polymer-based lens and the axis paper is 7.5 cm, hence the image distance (i) is 7.5 cm.

Using the Thin Lens Equation with known the object distance (o) of 44.0 cm and the focal length (f) of 6.0 cm, the theoretical image distance (i) is 6.95 cm. Comparing with the image distance (i) of 7.5 cm obtained for the experiment, these two distances fit well. A type of lens created from thermally deforming polymer was theoretically confirming with the Thin Lens Equation.

3.2.6 Optics Lab Modelling for Light Concentrating Process

In order to understand the lensing properties of this polymer deformable lens, Optics Lab software is applied to model this LED light concentrating process. Optics Lab is a ray tracing program for optical design and analysis. With this software, two convex lenses with each diameter of 28 mm and focal length (f) of 60 mm were modelled and partly overlapped for simulating the polymer deformable lens. The center thickness of

each lens is 0.50 mm (reading from the polymer surface profile measurement) with a material refractive index of 1.5. At the object distance (o) of 440 mm away from the lenses, one light source was simulated to emit light, travel through the lenses and illuminate the screen on the bottom at the image distance (i) of 75 mm. A simulated schematic is shown in Figure 52.

Table 4: The simulated light source parameters in Optics Lab.

Source Parameters	
Number of rays	17 (1D)
Size of source	60 mm
Radius of curvature	0 mm
Radiation direction	90˚ rotation (in plane)
Index of refraction	1.00
Power emitted per source	1.00 W

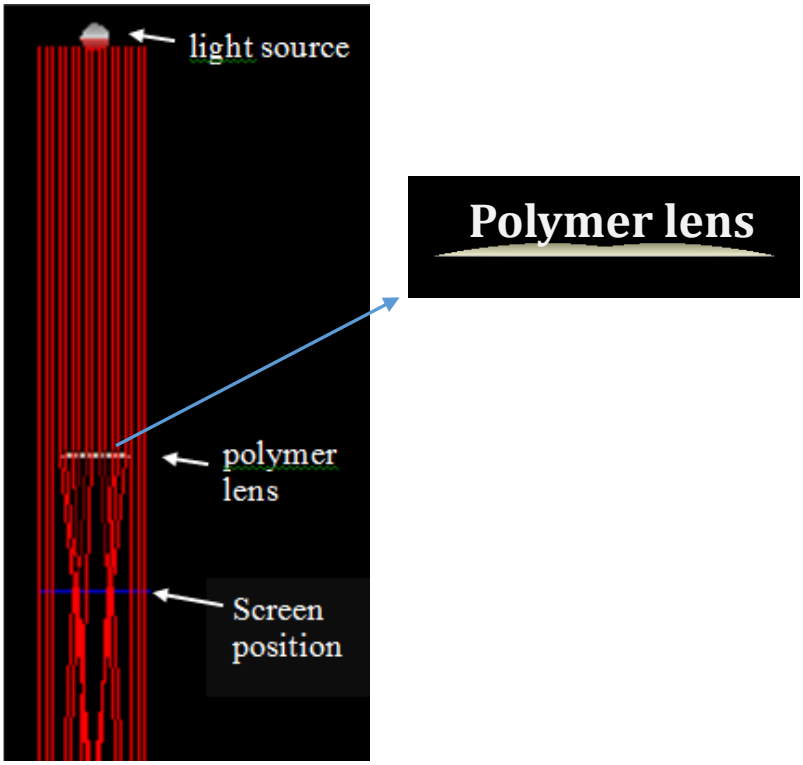

Figure 52: Schematic figure from Optics Lab to show the principle of light concentrating by polymer deformable lens.

As can be clearly shown in Figure 52, when the light emitted from the light source on the top, reaches the lenses, these lenses act to focus light into two beams, and the focal point was correctly located at the screen position.

3.2.7 Weight loss of solvent in polymer layer

Before and after each ITO stripe heat-treatment experiment, the weight of the same polymer sample was observed to be different and the vaporized organic solvent cooled down and deposited on the top glass of the sealed glass chamber after each experiment.

In order to test the cycle repeatability of the polymer deformable lens (to determine whether it has the ability to form a thermally generated lens when heated and then transform into a flat surface when cooled down), the polymer sample after lens formation

was heated at 150 ℃ for 15 minutes with a hot plate, and returned to a flat surface with some bubbles. Then the second attempt to form lenses with an ITO stripe heating source with that polymer sample was conducted. The polymer surface remained flat without any light focusing results observed. This polymer sample cannot be reusable for generating lenses. The main reason is the vaporizing loss of solvent in the polymer layer [40].

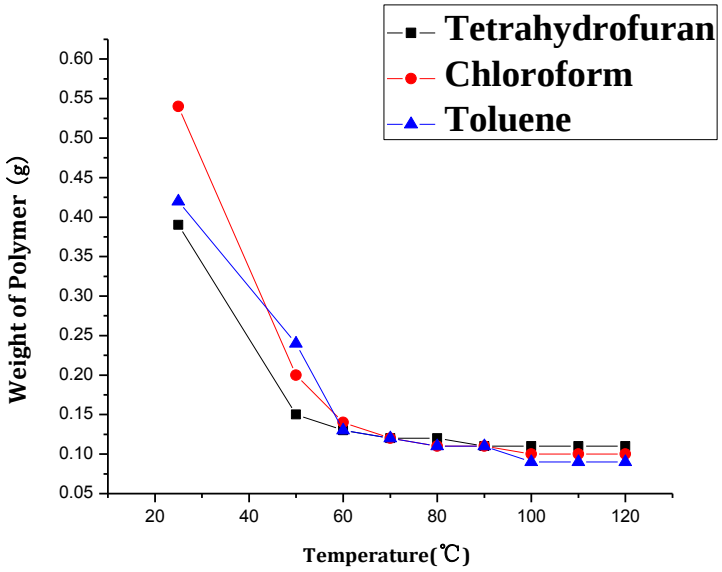

Figure 53: The weight of polymer samples at different temperature.

To analyse the loss of solvent, starting from different weight of polymer samples with three kinds of organic solvents at room temperature, these samples were losing weight with increasing the temperature because of the vaporization of the solvent in each polymer sample. The weight of all polymer samples became stable at 100 ℃, at which the organic solvents in these polymer samples have ceased vaporizing.

Table 5: The weight loss of polystyrene (PS) with three kinds of organic solvent before and after 18 hours ventilation.

Solvent	Toluene	Tetrahydrofuran	Chloroform
Weight of PS	0.12g	0.12g	0.11g
Weight of Solvent Before 18 hours	0.30g	0.27g	0.43g
Weight of Polymer sample After 18 hours	0.13g	0.13g	0.14g

According to the mass ratio of the polymer solution, the weight of polystyrene and solvent in the polymer sample cast on the glass surface can be calculated separately. From Table 5 above, it can be observed clearly that vaporization of the organic solvent in all three polymer samples almost stopped after 18 hours ventilation in the fume hood.

Combing the 18 hours ventilation with the temperature 100 ℃ at which the weight of polymer samples became stable, the solvent percentage in the polymer layer before the experiment can be determined.

Table 6: The solvent percentage in the polymer layers before the experiment.

Weight of Polymer sample	Toluene	Tetrahydrofuran	Chloroform
After 18 hours (W_1)	0.0654g	0.0972g	0.1172g
Heating at 100℃for 15min (W_2)	0.0604g	0.0899g	0.0999g
Solvent Weight Percentage $(W_1-W_2)/W_1$	7.6%	7.5%	14.8%

Comparing with the starting mass fraction of solvent in the polymer solution (63.0% with toluene, 64.3% with tetrahydrofuran and 75.0% with chloroform) based on the mass ratio of prepared polymer solution (Polystyrene (1): Toluene (1.7), Polystyrene (1): Tetrahydrofuran (1.8), and Polystyrene (1): Chloroform (3.0)), the vaporization of organic solvents in the polymer layers before the thermal generating lens experiment is serious. High vaporization of the organic solvent will not only decrease of the utility of this polymer-based device in the actual application, but pollute the environment.

The high vaporization rate can also be observed with polymer samples before and after the thermal generating lens experiment and 5 days recording of the weight change of the polymer layer.

Table 7: The solvent weight loss of Polystyrene with Tetrahydrofuran and Chloroform polymer samples before and after thermal generating lens experiment on the different ITO stripe width heating source at various voltage.

Solvent	Tetrahydrofuran	Chloroform
7V 2mm	0.237%	0.112%
8V 2mm	0.290%	1.03%
9V 2mm	0.449%	0.497%
7V 6mm	0.352%	1.089%
8V 6mm	0.588%	1.130%
9V 6mm	1.719%	6.810%
7V 10mm	0.706%	2.274%
8V 10mm	0.951%	2.309%
9V 10mm	2.320%	5.667%

The solvent loss percentage of chloroform is higher than that of tetrahydrofuran because of the higher vapor pressure. Comparing with the solvent percentage of the polymer samples before the experiment, the organic solvent vaporized substantially through the experiment process.

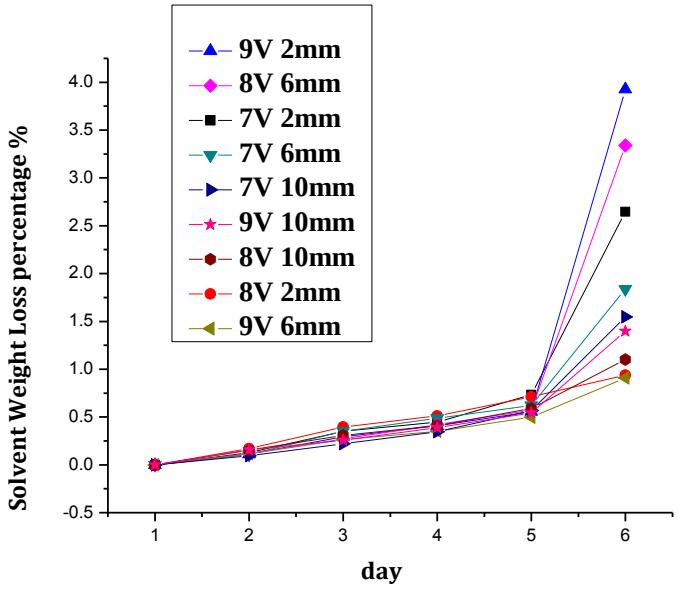

Figure 54: The solvent weight loss of Polystyrene with Tetrahydrofuran polymer samples during 5 days and heating at 100 ℃ for 15 minutes at the 5th day.

The vaporization of the organic solvent was still in progress even after the 5th day comparing to the 1st day and because of different weight at the beginning for all these polymer samples, the solvent weight loss percentage is slightly different, however, all the samples follow the same trend of vaporization. After 5 days, polymer samples were heated at 100 ℃ for 15 minutes to release the remaining unstable organic solvent. There was still 1% ~ 2.7% of organic solvent vaporized.

3.2.8 Reversing ITO Heating Source with The Polymer Layer on The Bottom

To determine the effect of the heating source position on the focal properties and the major role of two formation theories (Rayleigh-Bénard convection and Bénard-Marangoni flow effect), the experiment with polymer layer (polystyrene with toluene solvent) on the bottom of the 6 mm stripe width ITO heating source at 8 V was conducted.

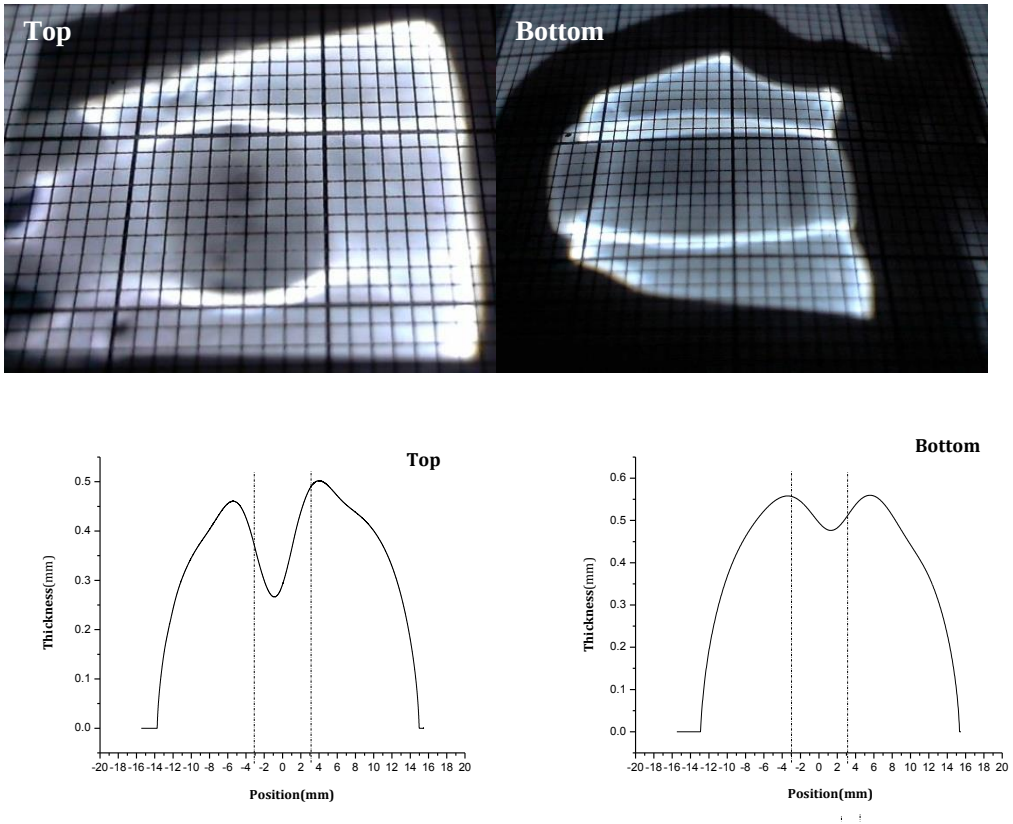

Figure 55: Light focusing image and surface profile of Polystyrene with Toluene generating lens on the top surface of 6 mm stripe width ITO heating source at 8 V and reversing ITO heating source with polymer layer on the bottom.

When reversing the ITO coated glass with the polymer layer on the bottom, the gravity slightly impeded the formation of a thermally generating lens, and the smaller

valley between two bumps can be seen in the surface profile of the reversed samples with polymer layer on the bottom.

However, similar light focusing image were obtained through these two polymer samples, the two sharp lines and similar distance between these two lines could confirm that Bénard-Marangoni flow effect by surface tension gradient decreasing from the center to the side made a dominant contribution to the formation of the polymer-based lens [41].

For better light focusing results and actual application in the future, the ITO coated glass heating source should ideally be horizontal to prevent gravity from impeding the formation of this thermally generating lens.

Chapter 4: Conclusions and Future Work

4.1 Summary

This research demonstrated transport of luminescent particles for possible application to fluorescent solar concentrators (FSCs). In addition this research demonstrated an optical lens generated from a thermally deformed polymer.

FSCs consist of fluorescent materials embedded in a substrate that absorb and emit light which is then concentrated within a fluorescent waveguide and guided to its edges to be absorbed by edge-mounted solar cells. A higher efficiency process of absorbing and guiding the light can be realized if the fluorescent materials have the ability to move following the position of the sun. By eliminating the need for a high-cost mechanical system for the movement of fluorescent materials, we can decrease the expense and also increase the efficiency of the FSCs system.

Because of a high-cost issue brought about by the use of large areas of solar panels in order to absorb significant amounts of sunlight, a novel type of low-cost lens can move to follow the sun. Instead of big optical glass lenses or other types of solar concentrator designs, the required area of solar panels can be decreased using low cost lenses focusing the sunlight wherever the sun is during the daytime.

For these purposes, both types of research are focusing on the more efficient utility of light with low-cost polymer-based devices and in particular by harnessing their unique thermal properties.

4.1.1 The Movement of YAG:Ce on Melted Polymer

From the laser-based wetting angle measurement, the hot melt glue stick have a larger wetting angle on the surface of the glass substrate and therefore the ability to transport particles along the melt polymer upon heating can be achieved. The transport of YAG:Ce was observed with hot melt glue stick however it was not observed using other polymers low melting point polymers such as crystal bond during the experiment.

In this experiment, the floating YAG:Ce at the surface of the liquid polymer can be pushed forward by two bumps or raised areas formed by surface tension differences caused from the thermal gradient by the hot wire on the top of the melted glue stick polymer. Because the one raised area was supporting the YAG:Ce particles in the experiment, the observed movement of the said one raised area can follow the wave movement of the melted polymer surface, resulting in the transport of YAG:Ce particles as well.

Because of the high vaporization rate of the polymer when heated, one PVB (Polyvinyl butyral) layer from DuPont® was heat-treated with a digital hot plate and the weight loss as a function of the increasing temperature was measured. Starting from room temperature, the opaque PVB film began losing weight and becoming optically clear at around 70 ℃. When the temperature reaching 120 ℃, the PVB film started to melt, followed by the colour changing from clear to yellow and burning at 150 ℃.

The thermal conductivity of glass of 0.8 $W\ m^{-1}\ K^{-1}$ at 293 K is still high, compared to the Polytetrafluoroethylene, Teflon (PTFE) value of 0.25 $W\ m^{-1}\ K^{-1}$ at 293 K. The glass cracking problem when the polymer layer on the top of it cooled down was also

observed during the experiment. Hence, one piece of Teflon sheet (thickness of 2 mm) was used for the polymer heat-treated trial. The desired result was obtained without a substrate cracking problem and low excessive heat dissipation was ensured.

4.1.2 The Polymer-Based Deformable Lens for Solar Tracking

The focal property of the polymer-based deformable lens is highly dependent on the surface tension difference caused by the thermal gradient from the center to the side where the ITO glass heating source was located. So the surface temperature profile of the ITO heating source was measured with a J-type thermocouple with a diameter of 76.2 μm. The temperature increased with the increasing ITO stripe width and heating power, and decreased from the center to the side, which formed a thermal gradient, resulting in a surface tension gradient.

Using the COMSOL Multiphysics modelling software, a heating source (modelled as a heat flux) with widths of 2 mm, 6 mm and 10 mm and height of 1 mm (the glass substrate thickness) at different heating powers was modelling in 2D view. We observed the same trend of surface temperature change with the measurement. However, the modelled temperatures were higher than the experimental measurements, and the temperature gap between the modelling reading and experimental measurement also increased with increasing heating power and ITO stripe width.

From the light focusing image of Polystyrene with toluene solvent, the focusing line becomes sharp and brighter with higher voltage. For the 2 mm ITO stripe at all voltages, no obvious light focusing results were obtained. The heated polymer has flowed further at 9 V than it did at lower voltages, and the polymer spread in a disorderly manner with

unexpected light focusing regions, which was proved by the resulting polymer surface profile: the deeper valley was observed from the polymer-based lens sample on the wider ITO stripe at a higher voltage and no obvious valley occurs for the polymer on the 2 mm width ITO stripe.

The same trend occurred with the polystyrene having toluene solvent. However, different diameters of bubbles formed during the heating process, scattering severely light transmission, and the same bubbles occurred in the polymer sample consisting of the polystyrene and chloroform.

The polymer flow relies on the dilution effect by the solvent in the polymer during heating. Starting from a smooth cast polymer of uniform thickness, the polymer-based lens containing two bumps is generated by the combination of Rayleigh-Bénard convection and Bénard-Marangoni flow effects.

Based on the original surface profile of the polystyrene-toluene polymer sample, the focal length (f) is 60 mm, half of the lens radius of curvature of 120 mm, and the image distance (i: the distance between the lens and the screen) of 7.5 cm was determined when the peak luminance indicating focusing of the sharp line is the highest reading from the photometer. Using the Thin Lens Equation, the theoretical image distance (i) is 6.95 cm, and both image distances from the experiment and the equation fit well. A type of lens created from the thermally deforming polymer was shown to confirm the Thin Lens Equation, which was also confirmed with Optics Lab modelling software. In this ray tracing modelling, when the light emitted from the light source reached the surface of the

lenses, these lenses act to focus light into two beams, and the focal point was correctly located at the screen position.

The solvent percentage in the polymer layer before the heat-treatment experiment (Polystyrene with toluene (7.6%), Polystyrene with tetrahydrofuran (7.5%), and Polystyrene with chloroform (14.8%)) was much lower compared with the starting mass ratio of the polymer solution (Polystyrene with toluene (63.0%), Polystyrene with tetrahydrofuran (64.3%), and Polystyrene with chloroform (75.0%)) because of the high vaporization of the organic solvent. The organic solvent also vaporized substantially through the experimental process. After 5 days of room temperature vaporization, there were still 1% ~ 2.7% of organic solvent vaporized as a weight percentage of the polymer layers, which were actually heated by ITO before being left for 5 days.

These polymer samples that had lost solvent were no longer usable for generating lenses.

The Bénard-Marangoni flow effect made a greater contribution to the formation of the polymer-based lens confirmed by the two sharp lines and similar distance between these two lines with the regular focal image when reversing the ITO coated glass with the polymer layer on the bottom.

4.2 Future Research

Because of the inaccuracy existing in the wetting angle measurement, such as the reading of laser dot position subject to human error, a more precise method is required for obtaining the in-situ surface profile of the melted polymer through the experimental process. A more suitable substrate for this experiment having low thermal conductivity

and high-stress resistance, and also an optically clear property, which is required for light collection would be ideal for future work.

Thermal modelling needs to be more carefully connected to the experimental apparatus, by including more precise surface and surrounding heat transfer parameters and the heat generation method. Also the surface temperature profile measurement needs to be modified as well.

The chosen solvent for polymer casting with more suitable properties (low vapor pressure) is a requirement for reversible thermally formable lenses. For better light focusing results and actual application in the future, the heat source should be horizontal to prevent gravity from impeding the formation of this thermally generating lens.

This project was concluded without the application of these two kinds of material devices into the actual solar application. Integration of the YAG:Ce transport processes into a concentrating fluorescent solar collector and the thermally generated polymer lens for a sunlight focusing and tracking system is the final goal of this research.

References

[1] "Solar Power 2014-Still Growing, Still Niche," The Lukewarmer's Way, [Online]. Available: https://thelukewarmersway.wordpress.com/2015/02/05/solar-power-2014-still-growing-still-niche/.

[2] D. Rahm, "Climate Change Policy in the United States: The Science, the Politics and the Prospects for Change," McFarland & Company, Inc. Publishers, San Marcos, TX (2009), pp. 150 - 152.

[3] "Solar panels connect to base electric grid," Nellis Air Force Base, [Online]. Available: http://www.nellis.af.mil/news/story.asp?id=123071269.

[4] "Sun tracking systems," Schmid Pekintas Energy Inc, [Online]. Available: http://www.schmid-pekintas.com/sun-follow.php.

[5] V. Sark, "Luminescent Solar Concentrators," Renew. Energ. **2013**, 207 - 210 (2012).

[6] V. Sholin, J. Olson and S. Carter, "Semiconducting polymers and quantum dots in luminescent solar concentrators for solar energy harvesting," J. Appl. Phys. **101**, 1 - 9 (2007).

[7] F. Muhammad-Sukki, R. Ramirez-Iniguez, S. McMeekin, B. Stewart and B. Clive, "Solar Concentrators," Int. J. Appl. Sci. **1**, 1 - 15 (2010).

[8] Y. Yuan and T. R. Lee, "Chapter 1 Contact Angle and Wetting Properties," in "Surface Science Techniques," Springer-Verlag Berlin Heidelberg Publishers, Houston, TX (2013), pp. 3 - 6.

[9] S. R. Palit, "Thermodynamic Interpretation of the Eötvös Constant," Nature **177**, 1180 (1956).

[10] "Surface Tension by the Ring Method (Du Nouy Method)," PHYWE, [Online]. Available: http://www.nikhef.nl/~h73/kn1c/praktikum/phywe/LEP/Experim/1_4_05.pdf.

[11] "Physical Properties Sources Index: Eötvös Constant," Chemistry Biology Pharmacy Information Center, [Online]. Available: http://www.ppsi.ethz.ch/fmi/xsl/eqi/eqi_property_details_en.xsl?node_id=1113.

[12] W. J. Moore, "Physical Chemistry Third Edition," Prentice-Hall, Inc. Publishers,

London, England (1957).

[13] "Rayleigh-Benard Convection," UC San Diego, Department of Physics, [Online]. Available: http://web.archive.org/web/20090222182327/http://physics.ucsd.edu/was-daedalus/convection/rb.html.

[14] A. V. Getling, "Rayleigh-Bénard Convection: Structures and Dynamics," World Scientific Publishing Co. Pte. Ltd. Publishers, Singapore (1998).

[15] N. Bassou and Y. Rharbi, "Role of Bénard-Marangoni Instabilities during Solvent Evaporation in Polymer Surface Corrugations," Langmuir **25**, 624 - 632 (2009).

[16] J. L. Mcgrew, T. L. Rehm, and R. G. Griskey, "The Effect of Temperature Induced Surface Tension Gradients on Bubble Mechanics," Appl. Sci. Res. **29**, 195 - 196 (1974).

[17] Y. Sumino, N. Magome, T. Hamada and K. Yoshikawa, "Self-Running Droplet: Emergence of Regular motion From Nonequilibrium Noise," Phys. Rev. Lett. **94**, 1 - 4 (2005).

[18] "Semiconductor Wafer Cleaning and Drying," [Online]. Available: http://solutions.3mphilippines.com.ph/wps/portal/3M/en_PH/3MNovec_APAC/Home/Applications/SemiconductorCleaning/WaferCleaningDrying/.

[19] "9. Marangoni Flows," MIT OpenCourseWare, [Online]. Available: http://ocw.mit.edu/courses/mathematics/18-357-interfacial-phenomena-fall-2010/lecture-notes/MIT18_357F10_Lecture9.pdf.

[20] B. Wunderlich, "Crystal Melting," in "Macromolecular Physics," Academic Press Publishers, New York, NY (1980), pp. 363.

[21] Z. Y. Liu, S. Liu, K. Wang and X. B. Luo, "Status and prospects for phosphor-based white LED packaging," Front. Optoelectron. **2**, 119 - 140 (2009).

[22] Z. Y. Liu, S. Liu, K. Wang and X. B. Luo, "Optical analysis of colour distribution in white LEDs with various packaging methods," IEEE Photonic. Tech. Lett. **24**, 2027 - 2029 (2008).

[23] S. C. Allen and A. J. Steckl, "A nearly ideal phosphor-converted white light-emitting diode," Appl. Phys. Lett. **92**, 1 - 3 (2008).

[24] "Polystyrene resin prices jump," Crain Communications Inc., [Online]. Available: http://www.plasticsnews.com/article/20140116/NEWS/140119947/polystyrene-resin-prices-jump.

[25] J. Maul, B. G. Frushour, J. R. Kontoff, H. Eichenauer, K. -H. Ott and C. Schade, "Polystyrene and Styrene Copolymers," in "Ullmann's Encyclopedia of Industrial Chemistry," Wiley-VCH Publishers, Weinheim (2007).

[26] "Common Plastic Resins Used in Packaging," Introduction to Plastics Science Teaching Resources, American Chemistry Council, Inc., [Online]. Available: http://plastics.americanchemistry.com/Education-Resources/Hands-on-Plastics/Introduction-to-Plastics-Science-Teaching-Resources/History-of-Polymers-Plastics-for-Teachers.html.

[27] E. Hecht, "Optics Second Edition," Addison Wesley Publishers, Boston, MA (1987).

[28] Materials properties of thermocouple wires sold by Omega Engineering, Inc. [Online]. Available: http://www.omega.com/.

[29] S. Sen, B. K. Dhindaw, D. M. Stefanescu, A. Catalina and P. A. Curreri, "Melt Convection Effects On the Critical Velocity of Particle Engulfment," J. Cryst. Growth **173**, 574 - 584 (1997).

[30] H. Kim, C. M. Gilmore, A. Piqué, J. S. Horwitz, H. Mattoussi, H. Murata, Z. H. Kafafi and D. B. Chrisey, "Electrical, optical, and structural properties of indium - tin - oxide thin films for organic light-emitting devices," J. Appl. Phys. **86**, 1 - 11 (1999).

[31] Kitai, A. (2014), 4L04 Spin on Application of Glass and Polymer Films [Online]. Available: http://coursenotes.mcmaster.ca/4L04/Thin_Films/Spin-on_Application_of_Glass_and_Polymer_Films.pdf.

[32] Kitai, A. (2014), 4L04 Oxidation Growth of SiO_2 on Silicon [Online]. Available: http://coursenotes.mcmaster.ca/4L04/Thin_Films/Oxidation_Growth_of_SiO2_on_Silicon.pdf.

[33] Kitai, A. (2014), 4L04 Electrodeposition of Metal [Online]. Available: http://coursenotes.mcmaster.ca/4L04/Thin_Films/Electrodeposition_of_Metal.pdf.

[34] Sigma-Aldrich Corporation, [Online]. Available: http://www.sigmaaldrich.com/catalog/product/aldrich/331651?lang=en&region=CA.

[35] D. Ennis, H. Betz and H. Ade, "Direct Spincasting of Polystyrene Thin Films onto Poly(metyl methacrylate)," J. Polym. Sci. : Part B: Polym. Phys. **44**, 3234 - 3244 (2006).

[36] "Toluene, Tetrahydrofuran, Chloroform," [Online]. Available: https://en.wikipedia.org/wiki/Toluene, Tetrahydrofuran, Chloroform.

[37] D. Hugh, "HyperPhysics," in "University Physics, Seventh Edition," Addison Wesley Publisher, Boston, MA (1992).

[38] M. L. Hallensleben, "Polyvinyl Compounds, Others," in "Ullmann's Encyclopedia of Industrial Chemistry," Wiley-VCH Publishers, Weinheim (2010).

[39] The Engineering ToolBox, [Online]. Available: http://www.engineeringtoolbox.com/thermal-conductivity-d_429.html.

[40] P. G. de Gennes, "Instabilities During The Evaporation of A Film: Non-Glassy Polymer + Volatile Solvent," Eur. Phys. J. E **6**, 421 - 424 (2001).

[41] S. Sakurai, C. Furukawa, A. Okutsu, A. Miyoshi and S. Nomura, "Control of Mesh Pattern of Surface Corrugation via Rate of Solvent Evaporation in Solution Casting of Polymer Film in The Presence of Convection," Polymer **43**, 3359 - 3364 (2002).